

First-principles derivation of elastic interaction between Jahn-Teller centers in crystals via lattice Green's functions

Zhishuo Huang,^{1,*} Naoya Iwahara,² and Liviu F. Chibotaru^{3,†}

¹*Department of Chemistry, National University of Singapore, Block S8 Level 3, 3 Science Drive 3, Singapore 117543, Singapore*

²*Graduate School of Engineering, Chiba University, 1-33 Yayoi-cho, Inage-ku, Chiba 263-8522, Japan*

³*Theory of Nanomaterials Group, KU Leuven, Celestijnenlaan 200F, B-3001 Leuven, Belgium*

(Dated: January 17, 2024)

Jahn-Teller (JT) systems with strong and intermediate vibronic coupling are described in terms of local JT active vibrational modes. In JT crystals, the elastic interaction of these modes at different JT centers plays a crucial role, for instance, in determining critical temperature of structural phase transitions. Despite their importance, the parameters of elastic interaction between JT centers have not been accessed yet by first-principles calculations. In this paper, we develop an effective Hamiltonian methodology for the thorough description of the elastic interactions in cooperative Jahn-Teller problems, which treats the interactions with both phonons and uniform strains. All the microscopic parameters, such as lattice Green's functions, elastic modulus, can be obtained or calculated based on first-principles calculation. The method has been applied to a series of $5d^1$ double perovskites. Such effective Hamiltonian methodology can be, in general, used to investigate the APES of any type of the local distortions, such as impurities, defects, etc.

I. INTRODUCTION

Multi-center vibronic interactions are found in a wide number of systems such as impurity Jahn-Teller (JT) centers [1], multi-center molecular clusters [2] and JT crystals [3, 4]. In these compounds, except for the $E \otimes b_1$, $E \otimes b_2$, and $T \otimes e$ the vibronic problem, where the vibronic interaction on the centers does not mix different electronic functions, the vibronic problem becomes rather involved, because the localized electrons in degenerated orbital states interact with the JT active distortions of the JT centers, while these JT centers interact via the common vibrational modes (phonons) of the system [5, 6].

Regarding the co-operative JT effect, an one-center nuclear coordinates based approach was proposed for the investigation of the adiabatic potential of molecular systems [7, 8]. However, such an approach seems to be less adequate in the case of two interacting Jahn-Teller impurities in the crystal, in which the derivation of the model Hamiltonian for the static JT effect [9] lack of substantiation. Another method, assuming that the displacement fields due to JT impurities are independent, has been developed, as a perfect approximation for the system where the JT impurities are sufficiently distant [10, 11]. Thus, the theory of vibronic interactions in these systems is not well-developed compared with one-center systems.

In this paper, with the microscopic parameters from first-principles calculations, an effective Hamiltonian for a static cooperative JT effect is proposed. This methodology is then applied to a series of double perovskites (DP) $A_2B'BX_6$.

B' -site ordered double perovskites, of which the structure is shown in Fig. 1 (a), have attracted increasing interests because of its potential to host diverse exotic states of matter [12]. Different combination of magnetic or nonmagnetic cations of A, B' and B sites will lead to different magnetic phases [13]. There are three series of these DP materials with B electronic configurations nd^1 (T_{2g}^1), nd^2 (T_{2g}^2), and nd^3 (T_{2g}^3), of which each series presents different issues. For example, the crystallographic distortions of T_{2g}^1 and T_{2g}^2 ions are potentially attributed to JT effect, while T_{2g}^3 ions are not. In addition, the orbital moment is not fully quenched in T_{2g}^1 and T_{2g}^2 ions while nd^3 ions are orbital singlets. Recent publications summarize in tabular form what is known about the T_{2g}^2 and T_{2g}^3 cases [14–16]. For the simplicity, $5d^1$ (T_{2g}^1) double perovskites will be the targeted materials for the application.

II. EFFECTIVE HAMILTONIAN FOR COOPERATIVE JAHN-TELLER EFFECT

The basic mechanism for the JT effect is the interaction between nuclei vibrations and the electronic states. For isolated JT active centers, the methodology is clear as discussed by plenty of articles [4, 17–19]. When the JT centers are embedded in crystals, the properties of nuclei vibrations and the electronic structure will be altered by the collective vibrations in the crystal and the symmetry of crystal field, respectively. The properties of one JT active centers may be influenced by the neighboring JT active centers or even the JT active centers far way via phonons. Therefore in the study of cooperative JT effect, the vibrational part should be substituted by the analysis of phonon properties. Specially, when the JT active

* zhishuohuang@gmail.com

† liviu.chibotaru@kuleuven.be

centers presenting in a crystal lattice have a sufficiently high concentration, the stability of the entire crystal can be destroyed, which leads to the uniform strains. Thus, the thorough understanding of cooperative JT effect in crystals should consist of the investigation of the phonon contribution (elastic interaction part) and the uniform strain contribution [5, 6].

A. Contribution from phonons

The potential energy of the Jahn-Teller crystal is described by the operator

$$\hat{H} = \sum_{\mathbf{k}j} \frac{1}{2} \omega_{\mathbf{k}j}^2 Q_{\mathbf{k}j} Q_{\mathbf{k}j}^* + \sum_{\mathbf{n}} \hat{U}_{vib}^{\mathbf{n}}(\{q_{\mu\Gamma\gamma}^{\mathbf{n}}\}) \quad (1)$$

where \mathbf{k} and j denote the wave vector and phonon branch, respectively, $Q_{\mathbf{k}j}$ is the phonon modes and $\omega_{\mathbf{k}j}$ the corresponding frequency. $\hat{U}_{vib}^{\mathbf{n}}$, expressed on the basis of a set of (pseudo)degenerate electronic functions localizing at the corresponding center, describes the vibronic interaction with local nuclear distortions, denoted by $q_{\mu\Gamma\gamma}^{\mathbf{n}}$, which transforms after irreducible representation Γ of the site symmetry group at the \mathbf{n} th site of the crystal lattice.

The adiabatic potential energy surface (APES) can be obtained by the summing up the diagonalized potential energy operator ($\hat{U}_{vib}^{\mathbf{n}}$) on each JT active centers [20], expressing as

$$U_{\alpha_1\alpha_2\dots} = \sum_{\mathbf{k}j} \frac{1}{2} \omega_{\mathbf{k}j}^2 Q_{\mathbf{k}j} Q_{\mathbf{k}j}^* + \sum_{\mathbf{n}} \epsilon_{\alpha_n}^{\mathbf{n}}(\{q_{\mu\Gamma\gamma}^{\mathbf{n}}\}) \quad (2)$$

where α_n numbers the eigenvalues of the vibronic operator at the \mathbf{n} th center.

Since the phonon modes $Q_{\mathbf{k}j}$ form a complete set basis for the lattice dynamics, as a complete set basis for the dynamics of local JT active centers, local JT active modes $\{q_{\mu\Gamma\gamma}^{\mathbf{n}}\}$ can be expressed by the the phonon modes by Van Vleck coefficient $a_{\mu\Gamma\gamma}^{\mathbf{n}}(\mathbf{k}j)$ [21] as:

$$q_{\mu\Gamma\gamma}^{\mathbf{n}} = \sum_{\mathbf{k}j} a_{\mu\Gamma\gamma}^{\mathbf{n}}(\mathbf{k}j) Q_{\mathbf{k}j}. \quad (3)$$

The APES extrema can usually be found by Lagrange multiplier. However, this method can only be applied straightforward for simple JT problem, such as $E \otimes b_1$, $E \otimes b_2$, $T \otimes e$, because in these systems, the non-adiabaticity is no longer important, resulting in the only shifts of equilibrium phonon coordinates. While when the interaction between different JT centers are not negligible, the eigen values $\epsilon_{\alpha_n}^{\mathbf{n}}$ are complicated functions of $Q_{\mathbf{k}j}$, which makes the extrema equations unsolvable for systems with a large number of vibrational modes. Good thing comes when comparing the applications of Lagrange multiplier[22] to both $\{Q_{\mathbf{k}j}\}$, $\{q_{\mu\Gamma\gamma}^{\mathbf{n}}\}$ based on the condition defined in Eq. 3. Due to the parity symmetry ($Q_{\mathbf{k}j} = Q_{-\mathbf{k}j}^*$) [23], the complex phonon coordinates

will not double the number of corresponding extrema equations from the Lagrange multiplier. Following the procedure in Appendix A, we have reduced the system of extrema equations for the sheet $U_{\alpha_1\alpha_2\dots}$ to a limited number of equations depending on one-center JT active modes:

$$\frac{\partial \epsilon_{\alpha_n}^{\mathbf{n}}(\{q_{\mu\Gamma\gamma}^{\mathbf{n}}\})}{\partial q_{\mu\Gamma\gamma}^{\mathbf{n}}} + \sum_{\mathbf{n}'\mu'\Gamma'\gamma'} K_{\mathbf{n}'\mu'\Gamma'\gamma'}^{\mathbf{n}\mu\Gamma\gamma} q_{\mu'\Gamma'\gamma'}^{\mathbf{n}'} = 0 \quad (4)$$

with

$$K = \Xi^{-1} \quad (5)$$

$$\Xi_{\mathbf{n}'\mu'\Gamma'\gamma'}^{\mathbf{n}\mu\Gamma\gamma} = \sum_{\mathbf{k}j} \frac{a_{\mu'\Gamma'\gamma'}^{\mathbf{n}'*}(\mathbf{k}j) a_{\mu\Gamma\gamma}^{\mathbf{n}}(\mathbf{k}j)}{\omega_{\mathbf{k}j}^2}. \quad (6)$$

Detailed analysis of Eq. 5 and Eq. 6 can be found as following.

1. Derivation of the effective force matrix

From the derivation of the effective Hamiltonian in Appendix. A, the matrix Ξ and K are connected via $K = \Xi^{-1}$. Due to the periodicity, all the relevant property should be treated in reciprocal space[24], though both K and Ξ describe the elastic property in real space. To distinguish the parameters in both reciprocal space and real space, we write $\Xi_{\mathbf{n}'\mu'\Gamma'\gamma'}^{\mathbf{n}\mu\Gamma\gamma}$, $K_{\mathbf{n}'\mu'\Gamma'\gamma'}^{\mathbf{n}\mu\Gamma\gamma}$ as $\Xi_{\mu'\Gamma'\gamma'}^{\mu\Gamma\gamma}(\mathbf{n})$, $\Xi_{\mu'\Gamma'\gamma'}^{\mu\Gamma\gamma}(\mathbf{n})$, because they are parameters depending on the distance between different JT active centers, while the corresponding matrix elements in reciprocal space are denoted as $\Xi_{\mu'\Gamma'\gamma'}^{\mu\Gamma\gamma}(\mathbf{k})$, $\Xi_{\mu'\Gamma'\gamma'}^{\mu\Gamma\gamma}(\mathbf{k})$.

First, the $\Xi_{\mu'\Gamma'\gamma'}^{\mu\Gamma\gamma}(\mathbf{n})$ should be transformed into its representation in reciprocal space,

$$\Xi_{\mu'\Gamma'\gamma'}^{\mu\Gamma\gamma}(\mathbf{k}) = \sum_{\mathbf{n}} \Xi_{\mu'\Gamma'\gamma'}^{\mu\Gamma\gamma}(\mathbf{n}) \exp(i\mathbf{k} \cdot \mathbf{n}). \quad (7)$$

Second, for each \mathbf{k} , the inverse matrix of $\Xi(\mathbf{k})$ is calculated, which is the elastic coupling matrix in reciprocal space, $K(\mathbf{k})$.

$$K(\mathbf{k}) = \Xi^{-1}(\mathbf{k}). \quad (8)$$

Third, the inverse Fourier transformation will be applied to get the elastic coupling matrix in real space,

$$K_{\mu'\Gamma'\gamma'}^{\mu\Gamma\gamma}(\mathbf{n}) = \frac{1}{N} \sum_{\mathbf{k}} K_{\mu'\Gamma'\gamma'}^{\mu\Gamma\gamma}(\mathbf{k}) \exp(-i\mathbf{k} \cdot \mathbf{n}). \quad (9)$$

Since the contribution of phonon (K and Ξ) and uniform strains (K' and Ξ') are independent degrees of freedom, the corresponding total matrix should be the summation of the independent contribution, as shown in Eq. 27 and Eq. 28, respectively. The procedure of the calculation of K matrix, as shown above, can be applied to either each contribution or the total matrix.

2. Lattice Green's functions

In general, the JT active modes are expressed as:

$$q_{\mu\Gamma\gamma}^{\mathbf{n}} = \sum_{\mathbf{n}'\kappa\alpha} c_{\mu\Gamma\gamma}(\mathbf{n} - \mathbf{n}', \kappa, \alpha) \tau_{\kappa\alpha}(\mathbf{n}') \quad (10)$$

where expansion coefficients $c_{\mu\Gamma\gamma}(\mathbf{n} - \mathbf{n}', \kappa, \alpha)$ are the displacement of atom κ involved in JT active mode $\mu\Gamma\gamma$, which are known for different basic geometries of the centers[4], $\tau_{\kappa\alpha}(\mathbf{n}')$ is the Cartesian displacement of the atom of type κ at the unit cell \mathbf{n}' of the crystal, α denotes the Cartesian axis (x, y, z). The presence of $\mathbf{n} - \mathbf{n}'$ in $c_{\mu\Gamma\gamma}(\mathbf{n} - \mathbf{n}', \kappa, \alpha)$ is due to the fact that there might be atoms from other unit cells involved in one JT center, as the case of the JT center in fcc alkali-doped fullerenes A_3C_{60} (A is the alkali atom) in which one JT center involves 74 atoms: 60 carbon atoms, 8 cubic alkali atoms, and 6 octahedral alkali atoms, while there are only 63 atoms in the primitive unit cell [25].

In practical, the direct data from the first-principles

calculations is the phonon dispersion or dynamic matrices, by which any local distortion can be expressed by the phonon modes as[23]:

$$\tau_{\kappa\alpha}(\mathbf{n}) = \frac{1}{\sqrt{NM_\kappa}} \sum_{\mathbf{k}j} e_{\kappa\alpha}^{\mathbf{k}j} Q_{\mathbf{k}j} \exp(i\mathbf{k} \cdot \mathbf{n}) \quad (11)$$

where \mathbf{k} and j denote the momentum and the branch of the phonon, M_κ is the mass of the κ atom, N is the number of the unit cells in the crystal, and $e_{\kappa\alpha}^{\mathbf{k}j}$ denotes the polarization vector. Substituting Eq. 11 into Eq. 10, and comparing it with Eq. 3, we can easily have the expression of the Van Vleck coefficient[21]:

$$a_{\mu\Gamma\gamma}^{\mathbf{n}}(\mathbf{k}j) = \sum_{\mathbf{n}'\kappa\alpha} \frac{c_{\mu\Gamma\gamma}(\mathbf{n} - \mathbf{n}', \kappa, \alpha)}{\sqrt{NM_\kappa}} e_{\kappa\alpha}^{\mathbf{k}j} \exp(i\mathbf{k} \cdot \mathbf{n}). \quad (12)$$

Substituting Eq. 12 into Eq. A6, we have the final expression for the Ξ matrix:

$$\Xi_{\mathbf{n}'\mu'\Gamma'\gamma'}^{\mathbf{n}\mu\Gamma\gamma} = \sum_{\mathbf{l}\mathbf{m}} \sum_{\kappa'\kappa} \sum_{\alpha\beta} c_{\mu'\Gamma'\gamma'}(\mathbf{n}' - \mathbf{l}, \kappa', \beta) c_{\mu\Gamma\gamma}(\mathbf{n} - \mathbf{m}, \kappa, \beta) G_{\kappa'\alpha, \kappa\beta}(\mathbf{m} - \mathbf{l}) \quad (13)$$

with $G_{\kappa'\alpha, \kappa\beta}(\mathbf{n})$ defined as:

$$G_{\kappa'\alpha, \kappa\beta}(\mathbf{n}) = \frac{1}{N} \sum_{\mathbf{k}j} \frac{e_{\kappa'\alpha}^{\mathbf{k}j*} e_{\kappa\beta}^{\mathbf{k}j}}{\sqrt{M_{\kappa'} M_\kappa} \omega_{\mathbf{k}j}^2} \exp(i\mathbf{k} \cdot \mathbf{n}). \quad (14)$$

This $G_{\kappa'\alpha, \kappa\beta}(\mathbf{n})$ is the LGFs [23, 26], which can be obtained from both calculations neuron scattering measurements. From the computational point of view, the LGFs connect the eigenvalues and eigenvectors from the first-principles phonon calculations to the elastic coupling matrix Ξ based on the local JT active modes. On the other hand, the inverse of the LGFs have the same physical meaning of the inter-atomic force constants (IFC) from the standard phonon calculations[27], which is generated from the calculation of the dynamic matrix in the reciprocal space for a grid points in the Brillouin zone (BZ)[28]. However, because of the fact that one JT center might involve more atoms in neighboring unit cells, the evaluation of the elastic coupling for a small grid of unit cells requires the IFC on a larger grid of unit cells. Direct calculation of IFC for larger grid of unit cells is expensive, while a more economic way goes from the IFC on a small grid points in BZ, of which the dynamic matrix is calculated by first-principles method, to generated all the dynamic matrix for a thorough sampling of BZ by Fourier transformation. From this thorough sampling of BZ, the LGFs thus can be computed.

3. Extrema of APES

The solution of Eq. 4 is the equilibrium values in the extrema points $q_{\mu\Gamma\gamma}^{(\mathbf{n},0)}$, which is expressed as:

$$Q_{\bar{\mu}\bar{\Gamma}\bar{\gamma}}^{(0)} = \frac{1}{\omega_{\bar{\mu}\bar{\Gamma}}^2} \sum_{\mathbf{n}\mu\Gamma\gamma} a_{\mu\Gamma\gamma}^{\mathbf{n}}(\bar{\mu}\bar{\Gamma}\bar{\gamma}) \sum_{\mathbf{n}'\mu'\Gamma'\gamma'} K_{\mathbf{n}'\mu'\Gamma'\gamma'}^{\mathbf{n}\mu\Gamma\gamma} q_{\mu'\Gamma'\gamma'}^{(\mathbf{n}',0)} \quad (15)$$

with the stabilization energy as:

$$U_{\alpha_1\alpha_2\dots} = \sum_{\mathbf{n}\mu\Gamma\gamma} \sum_{\mathbf{n}'\mu'\Gamma'\gamma'} \frac{1}{2} K_{\mathbf{n}'\mu'\Gamma'\gamma'}^{\mathbf{n}\mu\Gamma\gamma} q_{\mu\Gamma\gamma}^{(\mathbf{n},0)} q_{\mu'\Gamma'\gamma'}^{(\mathbf{n}',0)} + \sum_{\mathbf{n}} \epsilon_{\alpha_n}^{\mathbf{n}} (\{q_{\mu\Gamma\gamma}^{\mathbf{n}}\}). \quad (16)$$

In general, substituting of $q_{\mu\Gamma\gamma}^{(\mathbf{n},0)} q_{\mu'\Gamma'\gamma'}^{(\mathbf{n}',0)}$ by $q_{\mu\Gamma\gamma}^{\mathbf{n}} q_{\mu'\Gamma'\gamma'}^{\mathbf{n}'}$, the properties of static JT effect around the equilibrium of extrema can be represented, thus the effective Hamiltonian for the static JT effect in multi-center JT systems can be described by:

$$\hat{H} = \sum_{\mathbf{n}\mu\Gamma\gamma} \sum_{\mathbf{n}'\mu'\Gamma'\gamma'} \frac{1}{2} K_{\mathbf{n}'\mu'\Gamma'\gamma'}^{\mathbf{n}\mu\Gamma\gamma} q_{\mu\Gamma\gamma}^{\mathbf{n}} q_{\mu'\Gamma'\gamma'}^{\mathbf{n}'} + \sum_{\mathbf{n}} U_{\alpha_n}^{\mathbf{n}} (\{q_{\mu\Gamma\gamma}^{\mathbf{n}}\}). \quad (17)$$

It should be noted that, the basic idea of such effective Hamiltonian is the downfolding of all vibrational modes or phonons onto the JT active modes, which does not mean that the contribution from any other local distortions other than these JT active modes is zero. In one word, such effective Hamiltonian can be, in general, used

to investigate the APES of any type of the local distortions, such as impurities, defects, etc.

B. Contribution from uniform strain

When the concentration of JT centers are low, which means the bulk deformation has nothing to do with JT centers, the above derivation of the effective Hamiltonian is complete. On the other hand, low-symmetry structural phases of Jahn–Teller crystals can also influence the bulk deformations[5, 29]. Besides, the phonon states and energies should be a function of the strain, however, because of the problem of applying proper boundary conditions when the crystal is stained, it is useful to treat stain separately from the phonons[6]. However, as pointed out by Born and Huang[30], the uniform strains describing the bulk deformations of the crystal cannot be reduced to a combination of phonon modes. In the following we generalize the approach by taking into account the effects of uniform strains as an independent degree of freedom.

The elastic contribution from uniform strain to the potential energy U_{us} is[31]:

$$U_{us} = \frac{1}{2}NV_0 \sum_{\alpha\beta, \alpha'\beta'} C_{\alpha\beta, \alpha'\beta'} \varepsilon_{\alpha\beta} \varepsilon_{\alpha'\beta'} \quad (18)$$

where N denotes the number of sites, V_0 is the volume of unit cell, $\varepsilon_{\alpha\beta}$ and $C_{\alpha\beta, \alpha'\beta'}$ are general strains and elastic modulus constants with α, β representing the Cartesian index (x, y, z). The definition of $\varepsilon_{\alpha\beta}$ is the same as the definition in any text book:

$$\varepsilon_{\alpha\beta} = \frac{1}{2} \left[\frac{\partial u_\alpha(\mathbf{R})}{\partial R_\beta} + \frac{\partial u_\beta(\mathbf{R})}{\partial R_\alpha} \right], \quad (19)$$

where \mathbf{R} is an arbitrary point in the crystal with \mathbf{u} the displacement field. For uniform strains, the components $\varepsilon_{\alpha\beta}$ are constants throughout the crystal.

Same as the treatment of the phonon contribution in Sec. II A, the U_{us} can be expressed by the symmetrized strains and modulus by the transformation with respect to the irreducible representation Γ of the corresponding crystalline class as:

$$U_{us} = \frac{1}{2}NV_0 \sum_{\Gamma\gamma} C_{\Gamma\gamma} \varepsilon_{\Gamma\gamma}^2 \quad (20)$$

with the transformation for strain and modulus as:

The uniform strain can be symmetrized by the same transformation as the construction of JT active modes [31]:

$$\varepsilon_{\Gamma\gamma} = \sum_{\alpha\beta} \Upsilon_{\alpha\beta}^{\Gamma\gamma} \varepsilon_{\alpha\beta} \quad (21)$$

$$C_{\Gamma\gamma} = \sum_{\alpha\beta} \sum_{\alpha'\beta'} C_{\alpha\beta, \alpha'\beta'} \Upsilon_{\alpha\beta}^{\Gamma\gamma} \Upsilon_{\alpha'\beta'}^{\Gamma\gamma} \quad (22)$$

where $\Upsilon_{\alpha\beta}^{\Gamma\gamma}$ is the unitary transformation from the Cartesian coordinates to the symmetrized basis, and $\varepsilon_{\Gamma\gamma}$, $C_{\Gamma\gamma}$ are the symmetrized strain and the modulus, respectively.

Based on the Kanamori's work[32], the uniform strains can be included in the theory of cooperative JT effect as additional terms of vibronic interaction at each JT center. On the other hand, with the symmetrization procedure of general strain and modulus above, the local JT active modes, $\{q_{\mu\Gamma\gamma}^{\mathbf{n}}\}$, can be employed for the full description of the vibronic problems. Thus, the interaction with uniform strains can be included implicitly as additional terms in the Van Vleck expansion, Eq. 12, as independent degrees of freedom:

$$q_{\mu\Gamma\gamma}^{\mathbf{n}} = \sum_{\mathbf{k}j} a_{\mu\Gamma\gamma}^{\mathbf{n}}(\mathbf{k}j) Q_{\mathbf{k}j} + \sum_{\Gamma'\gamma'} a_{\mu\Gamma\gamma}^{\mathbf{n}}(\Gamma'\gamma') \varepsilon_{\Gamma'\gamma'}. \quad (23)$$

Following the procedure as shown in Appendix B, the coefficients ($a_{\mu\Gamma\gamma}^{\mathbf{n}}(\Gamma'\gamma')$) of uniform strain contribution has the form:

$$a_{\mu\Gamma\gamma}^{us}(\Gamma'\gamma') = \sum_{\alpha\beta} \left[\sum_{\mathbf{n}'\kappa\alpha} c_{\mu\Gamma\gamma}(\mathbf{n} - \mathbf{n}', \kappa, \alpha) R_\beta(\mathbf{n}', \kappa) \right] (\Upsilon^{-1})_{\alpha\beta}^{\Gamma'\gamma'}. \quad (24)$$

Since the uniform strain is independent degrees of freedom, Eq. 6 can be employed directly with the coefficients defined as Eq. 24 for the potential contribution from uniform strain:

$$\Xi_{\mu'\Gamma'\gamma'}^{\mu\Gamma\gamma} = \sum_{\bar{\Gamma}\bar{\gamma}} \frac{a_{\mu'\Gamma'\gamma'}(\bar{\Gamma}\bar{\gamma}) a_{\mu\Gamma\gamma}(\bar{\Gamma}\bar{\gamma})}{V_0 C_{\bar{\Gamma}\bar{\gamma}}^0}. \quad (25)$$

Similar to the definition of elastic coupling matrix contributed from phonon, Eq. 5, the elastic coupling matrix contributed from the uniform strains, is calculation as:

$$K' = \Xi'^{-1}. \quad (26)$$

C. Total elastic interaction matrix

After the discussion about the two independent contributions for the elastic interaction for cooperative JT effect, we come to the total expression of the total elastic interaction matrix, expressing as:

$$\tilde{\Xi} = \Xi + \frac{1}{N} \Xi', \quad (27)$$

with Ξ , and Ξ' expressed by Eq. 13, and 25, respectively. The final expression of the elastic interaction for cooperative JT effect is reached as:

$$\tilde{K} = K + \frac{K'}{N}, \quad (28)$$

where the phonon contribution (K) and the contribution from uniform strains (K') are given by Eq. 5, and Eq. 26 respectively.

TABLE I. The crystal information of the $5d^1$ double perovskites. The space group is $Fm\bar{3}m$, with the Wyckoff position for atomic positions are A: $8c(1/4, 1/4, 1/4)$, B': $4b(1/2, 0, 0)$, B: $4a(0, 0, 0)$, and X: $24e(x, 0, 0)$,

A	B'	B	X	$A_2(B')BX_6$	Structure		Config
					$a/\text{\AA}$	$x(O)$	
Ba	Na	Os	O	Ba_2NaOsO_6 [33]	8.2870	0.2256	$5d^1$
	Li			Ba_2LiOsO_6 [33]	8.1046	0.2330	
	Mg	Re		Ba_2MgReO_6 [34]	8.0849	0.2392	
	Zn			Ba_2ZnReO_6 [35]	8.1061	0.23952	
	Y	W		Ba_2YWO_6 [36]	8.3848	0.2350	
Cs	Ta	Cl	Cs_2TaCl_6 [37]	10.2710	0.2331		
		Br	Cs_2TaBr_6 [38]	10.7685	0.2394		

III. COOPERATIVE JAHN-TELLER EFFECTS IN $5D^1$ DOUBLE PEROVSKITES

A. Crystal Structure and Jahn-Teller centers

The interested double perovskites in this paper are: Ba_2NaOsO_6 , Ba_2LiOsO_6 , Ba_2MgReO_6 , Ba_2ZnReO_6 , Cs_2TaCl_6 , Cs_2TaBr_6 and Ba_2YWO_6 , in which the B site are Ta^{4+} , W^{5+} , Re^{6+} , Os^{7+} , with the electron occupation situations $5d^1$ (T_{2g}^1). These double perovskites, $A_2B'BX_6$, crystallize into $Fm\bar{3}m$ crystals, with the point group O_h , as shown in Fig. 1 (a), with all the structure parameters shown in Table. I, of which the full list of atomic order is shown in Table. S1 in the supporting information. The structures are taken from the experiments, either determined by neutron powder diffraction or neutron powder refinements. However, not all x coefficient of these compounds were provided, such as of Cs_2TaBr_6 , and Ba_2YWO_6 , thus x coefficient of these materials were given as a general value, which was 0.2300, not far away from the real situation. A relaxation procedure with force convergence threshold 0.1 eV/Å was further performed to get a consistent x coefficient.

In this paper, all the calculations were performed for conventional unit cell, including four JT centers (Fig. 1 (b)). Each JT center consists of the $5d$ metal atom (Ta, W, Re, and Os) surrounded by six high electronegative atoms (O, Cl or Br), forming an octahedral configuration (1 (b)). The label and position of these JT centered atoms are listed in Table.II. The relative position of these four JT centers introduces two types of interacting pairs: one is interaction pair of JTC1 and JTC2, and the other one JTC1 and JTC4. Such an orientation of four JT centers need to be considered, however the analysis will be more complicated, which will be carried out in further studies. Thus in this paper, the relative orientation of the four JT centers will be ignored.

Since there is only one electron, due to the crystal field, the $5d$ orbital splits into E_g and T_{2g} , with E_g higher than T_{2g} . The JT involved orbitals are T_{2g} . The existence of spin-orbital interaction splits T_{2g} into

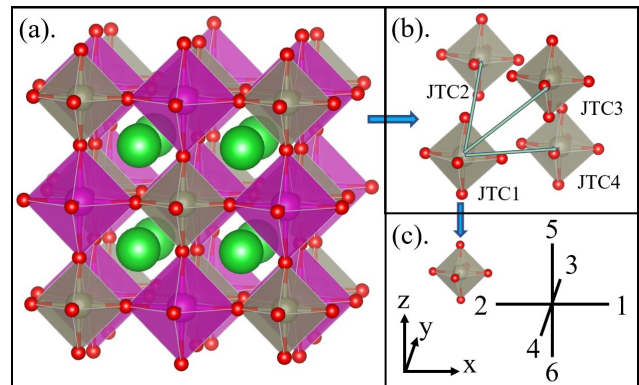


FIG. 1. The structure of double perovskites and configuration for Jahn-Teller center. (a). The crystal structure of double perovskite $A_2B'BX_6$, green, purple, grey, and red balls are A, B', B and X atoms, respectively. (b). The configuration of four JT centers in convention unit cell. (c). The coordinates and definition of one JT center. Detailed information of (b) and (c) can be found in Table. II.

TABLE II. Coordinates and symmetry adapted JT active modes, $q_{\mu\Gamma\gamma}$, of octahedral configuration. μ represents the position of JT center, labeled by JTC1 to JTC4 for the four JT centers in the convention unit cell, while $\Gamma\gamma$ distinguish JT active modes with the label JTD.1 to JTD.6, corresponding to a_{1g} , $e_{g\theta}$, $e_{g\epsilon}$, $t_{2g\xi}$, $t_{2g\eta}$, and $t_{2g\zeta}$.

JT active mode $q_{\mu\Gamma\gamma}$ for octahedral configuration							
Atoms	Position	a_{1g}	e_g		t_{2g}		
			θ	ϵ	ξ	η	ζ
		JTD.1	JTD.2	JTD.3	JTD.4	JTD.5	JTD.6
A1	(1,0,0)	$\frac{1}{\sqrt{6}}(1, 0, 0)$	$\frac{1}{2\sqrt{3}}(-1, 0, 0)$	$\frac{1}{2}(1, 0, 0)$	(0, 0, 0)	$\frac{1}{2}(0, 0, 1)$	$\frac{1}{2}(0, 1, 0)$
A2	(-1,0,0)	$\frac{1}{\sqrt{6}}(-1, 0, 0)$	$\frac{1}{2\sqrt{3}}(1, 0, 0)$	$\frac{1}{2}(-1, 0, 0)$	(0, 0, 0)	$\frac{1}{2}(0, 0, -1)$	$\frac{1}{2}(0, -1, 0)$
A3	(0,1,0)	$\frac{1}{\sqrt{6}}(0, 1, 0)$	$\frac{1}{2\sqrt{3}}(0, -1, 0)$	$\frac{1}{2}(0, -1, 0)$	$\frac{1}{2}(0, 0, 1)$	(0, 0, 0)	$\frac{1}{2}(1, 0, 0)$
A4	(0,-1,0)	$\frac{1}{\sqrt{6}}(0, -1, 0)$	$\frac{1}{2\sqrt{3}}(0, 1, 0)$	$\frac{1}{2}(0, 1, 0)$	$\frac{1}{2}(0, 0, -1)$	(0, 0, 0)	$\frac{1}{2}(-1, 0, 0)$
A5	(0,0,1)	$\frac{1}{\sqrt{6}}(0, 0, 1)$	$\frac{1}{2\sqrt{3}}(0, 0, 2)$	(0, 0, 0)	$\frac{1}{2}(0, 1, 0)$	$\frac{1}{2}(1, 0, 0)$	(0, 0, 0)
A6	(0,0,-1)	$\frac{1}{\sqrt{6}}(0, 0, -1)$	$\frac{1}{2\sqrt{3}}(0, 0, -2)$	(0, 0, 0)	$\frac{1}{2}(0, -1, 0)$	$\frac{1}{2}(-1, 0, 0)$	(0, 0, 0)
JT active center							
JTC1		(0, 0, 0)					
JTC2		(0, 0.5, 0.5)					
JTC3		(0.5, 0, 0.5)					
JTC4		(0.5, 0.5, 0)					

Γ_7 and Γ_8 . The low lying Γ_8 is the target orbital. The irreducible representation for this system is given as $\Gamma_{vib}^{oct} = a_{1g} \oplus e_g \oplus t_{2g} \oplus t_{1u} \oplus t_{2u}$, therefore according to selection rule, the Γ_8 orbitals linearly couple to JT active modes involved in the symmetric product of Γ_8 representation: $[\Gamma_8^2] = a_{1g} \oplus e_g \oplus t_{2g}$. a_{1g} will not be considered because of the fact that it only shifts the energy levels without any orbital splitting, thus all the parameters corresponding to a_{1g} will be ignored in the following analysis.

B. Computational methods

All the DFT calculations were performed by VASP[39–42]. The plane-wave kinetic energy cutoff was set

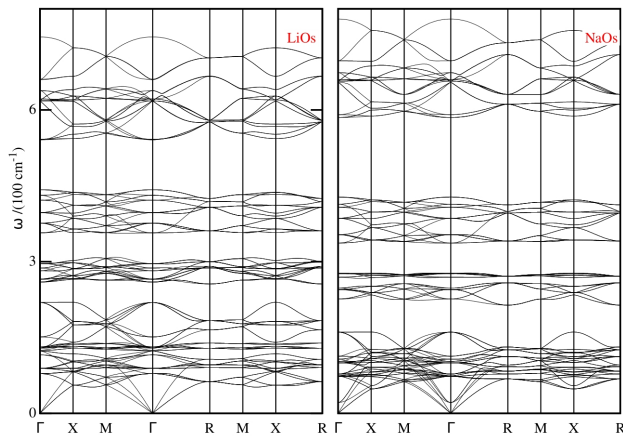


FIG. 2. Phonon dispersions of for $\text{Ba}_2\text{LiOsO}_6$ and $\text{Ba}_2\text{NaOsO}_6$, distinguished by ‘LiOs’ and ‘NaOs’, respectively.

to 400 eV for $\text{Ba}_2\text{NaOsO}_6$, $\text{Ba}_2\text{LiOsO}_6$, $\text{Ba}_2\text{MgReO}_6$, $\text{Ba}_2\text{ZnReO}_6$, and Ba_2YWO_6 , with 300 eV for Cs_2TaCl_6 , and Cs_2TaBr_6 , and a $6 \times 6 \times 6$ Monkhorst-Pack mesh was used to perform Brillouin zone (BZ) integration in order to ensure the convergence of self-consistent field calculation. The convergence threshold of total energy was set to 10^{-7} eV with that of the forces on atoms to 10^{-4} eV/Å for full relaxation calculations. Projector augmented-wave (PAW) pseudo-potentials [43, 44] are employed with the exchange and correlation approximations Generalized Gradient Approximation PBE (GGA-PBE) [45, 46].

The phonon calculations were carried out by frozen-phonon method with VASP+phonopy[47, 48], in which a $2 \times 2 \times 2$ super-cell was used, with the energy convergence threshold set as 10^{-9} eV. The LGFs are generated on a $31 \times 31 \times 31$, Monkhorst-Pack meshes in BZ. The elastic modulus was calculated by the density functional perturbation theory (DFPT)[49, 50], with a $12 \times 12 \times 12$ Monkhorst-Pack mesh to guarantee the convergence.

C. Ξ matrix

1. Phonon dispersion

The phonon dispersions of $\text{Ba}_2\text{LiOsO}_6$ and $\text{Ba}_2\text{NaOsO}_6$ are shown in Fig. 2, while the phonon dispersions of all the 7 double perovskites can be found in Fig.S1 in supporting information. $\text{Ba}_2\text{NaOsO}_6$ has more broadening dispersion than $\text{Ba}_2\text{LiOsO}_6$ because of the large ratio between the cations and anions. This is clearly from the phonon density of states (DOS), where O atoms mainly contribute to the high energy phonon DOS.

TABLE III. Ξ matrix for JT active centers in one convention unit cell. ‘PH’ and ‘US’ distinguish the parameters from phonons and uniform strain, respectively. From the left to right, and from the top to bottom, the matrix elements correspond to JTD_2, JTD_3, JTD_4, JTD_5 and JTD_6, respectively. The unit is bohr^2/Ha . ‘NaOs’ and ‘LiOs’ are for ‘ $\text{Ba}_2\text{NaOsO}_6$ ’ and ‘ $\text{Ba}_2\text{LiOsO}_6$ ’, respectively.

	NaOs	LiOs
$\begin{matrix} PH \\ (JTC1, JTC1) \end{matrix}$	$\begin{pmatrix} 4.988 & 0.000 & 0.000 & 0.000 & 0.000 \\ 0.000 & 4.988 & 0.000 & 0.000 & 0.000 \\ 0.000 & 0.000 & 10.472 & 0.000 & 0.000 \\ 0.000 & 0.000 & 0.000 & 10.472 & 0.000 \\ 0.000 & 0.000 & 0.000 & 0.000 & 10.472 \end{pmatrix}$	$\begin{pmatrix} 5.464 & 0.000 & 0.000 & 0.000 & 0.000 \\ 0.000 & 5.464 & 0.000 & 0.000 & 0.000 \\ 0.000 & 0.000 & 9.921 & 0.000 & 0.000 \\ 0.000 & 0.000 & 0.000 & 9.921 & 0.000 \\ 0.000 & 0.000 & 0.000 & 0.000 & 9.921 \end{pmatrix}$
$\begin{matrix} PH \\ (JTC1, JTC2) \end{matrix}$	$\begin{pmatrix} 0.065 & 0.035 & -0.037 & 0.000 & 0.000 \\ 0.035 & 0.025 & 0.065 & 0.000 & 0.000 \\ -0.037 & 0.065 & -0.200 & 0.000 & 0.000 \\ 0.000 & 0.000 & 0.000 & 0.058 & 0.025 \\ 0.000 & 0.000 & 0.000 & 0.025 & 0.058 \end{pmatrix}$	$\begin{pmatrix} 0.075 & 0.063 & -0.051 & 0.000 & 0.000 \\ 0.063 & 0.002 & 0.088 & 0.000 & 0.000 \\ -0.051 & 0.088 & -0.204 & 0.000 & 0.000 \\ 0.000 & 0.000 & 0.000 & 0.065 & 0.016 \\ 0.000 & 0.000 & 0.000 & 0.016 & 0.065 \end{pmatrix}$
$\begin{matrix} US \\ (JTC1, JTC1) \end{matrix}$	$\begin{pmatrix} 0.267 & 0.000 & 0.000 & 0.000 & 0.000 \\ 0.000 & 0.267 & 0.000 & 0.000 & 0.000 \\ 0.000 & 0.000 & 0.313 & 0.000 & 0.000 \\ 0.000 & 0.000 & 0.000 & 0.313 & 0.000 \\ 0.000 & 0.000 & 0.000 & 0.000 & 0.313 \end{pmatrix}$	$\begin{pmatrix} 0.386 & 0.000 & 0.000 & 0.000 & 0.000 \\ 0.000 & 0.386 & 0.000 & 0.000 & 0.000 \\ 0.000 & 0.000 & 0.243 & 0.000 & 0.000 \\ 0.000 & 0.000 & 0.000 & 0.243 & 0.000 \\ 0.000 & 0.000 & 0.000 & 0.000 & 0.243 \end{pmatrix}$
$\begin{matrix} US \\ (JTC1, JTC2) \end{matrix}$	$\begin{pmatrix} 0.033 & -0.081 & 0.000 & 0.000 & 0.000 \\ -0.081 & 0.127 & 0.000 & 0.000 & 0.000 \\ 0.000 & 0.000 & -0.016 & 0.000 & 0.000 \\ 0.000 & 0.000 & 0.000 & 0.148 & 0.000 \\ 0.000 & 0.000 & 0.000 & 0.000 & 0.148 \end{pmatrix}$	$\begin{pmatrix} 0.047 & -0.117 & 0.000 & 0.000 & 0.000 \\ -0.117 & 0.182 & 0.000 & 0.000 & 0.000 \\ 0.000 & 0.000 & -0.013 & 0.000 & 0.000 \\ 0.000 & 0.000 & 0.000 & 0.115 & 0.000 \\ 0.000 & 0.000 & 0.000 & 0.000 & 0.115 \end{pmatrix}$

2. Ξ matrix from phonons

The key parameters in phonon calculation are the IFCs, which describes the response property of one atom with respect to another atom in the crystal. The real space dimension of IFC corresponds to the super-cell generated in the phonon calculation procedure. From the IFCs, by Fourier transformation, the LGFs are generated. The Ξ matrix are computed by the LGFs and the JT active modes, defined in Table. II, by Eq. 13.

The calculated Ξ matrix is shown in Table. III. The onsite coupling parameters are diagonal and have a two and three degeneracy, corresponding to the E_g and T_{2g} states.

3. Ξ matrix from uniform strain

The evaluation of Ξ matrix from uniform strain are carried out with Eq. 25. The required parameters, such as volumes of the convention unit cell and the elastic modulus are listed in Table. IV. The Ξ matrix for $\text{Ba}_2\text{NaOsO}_6$ and $\text{Ba}_2\text{LiOsO}_6$ from the uniform strain, are shown in Table. III. Similarly to that of phonon, the Ξ matrix of uniform strain for the onsite JT center is diagonal with two and three degeneracy. Besides, they have the same magnitude order. However, the LGFs are generally expected to decrease fast with the distance between the centers, as $(\mathbf{n} - \mathbf{n}')^{-3}$ [51], so as the Ξ matrix. While the contribution from uniform strains remains constant for any distance between JT centers. Therefore phonons and uniform strains contribute comparably to the interaction energy of a given JT center with all other centers of the crystal. From this aspect, it is important to include the influence of uniform strain for Cooperative JT

TABLE IV. The volume V_0 (1000 \AA^3) and three independent general modulus, C_{xxxx} , C_{xxyy} , and C_{xyxy} (10^3 kBar) as well as the corresponding symmetrized three independent modulus, C_{A_1} , C_{E_θ} , and $C_{T_2(\xi)}$. ‘LiOs’, ‘NaOs’, ‘MgRe’, ‘ZnRe’, ‘YW’, ‘TaCl’, and ‘TaBr’ represent for $\text{Ba}_2\text{NaOsO}_6$, $\text{Ba}_2\text{LiOsO}_6$, $\text{Ba}_2\text{MgReO}_6$, $\text{Ba}_2\text{ZnReO}_6$, Cs_2TaCl_6 , Cs_2TaBr_6 , and Ba_2YWO_6 .

	V_0	C_{xxxx}	C_{xxyy}	C_{xyxy}	C_{A_1}	C_{E_θ}	$C_{T_2(\xi)}$
NaOs	0.5691	2.291	0.727	0.668	3.746	1.564	2.672
LiOs	0.5323	2.027	0.921	0.878	3.868	1.106	3.512
MgRe	0.5285	2.889	1.115	1.133	5.119	1.774	4.532
ZnRe	0.5326	2.678	1.340	1.022	5.358	1.338	4.088
TaCl	1.0835	0.264	0.126	0.106	0.516	0.139	0.426
TaBr	1.2487	0.203	0.101	0.088	0.405	0.101	0.352
YW	0.5895	3.603	0.943	0.811	5.489	2.661	3.245

effect.

D. Effective elastic coupling matrix K

Based on the method described in Sec. II A 1, the effective elastic coupling matrix, K , can be obtain for both phonons and uniform strains.

Though there are two types JT active modes (E_g , and T_{2g}) on each JT center, only E_g modes are considered, as the vibronic coupling constants of E_g are 6 times larger than that of T_{2g} according to N. Iwahara’s study[52], meaning that the contribution of E_g to JT energy is 36 larger than that of T_{2g} . Thus in the analysis of elastic coupling constants, T_{2g} JT active modes are ignored for simplicity.

In the previous section, $\Xi_{\mu'\gamma'}^{\mu\gamma}(\mathbf{R})$ (μ, μ' donate the four JT centers, γ, γ' donate the two components, θ, ϵ of E_g JT active mode, and \mathbf{R} represents the lattice vector) has been truncated to the 4th next nearest conventional unit cells, due to the fast decay of $\Xi_{\mu'\gamma'}^{\mu\gamma}(\mathbf{R})$ on \mathbf{R} . Thus, the elastic coupling matrix K can also be obtained for up to the 4th next nearest conventional unit cells.

The K matrix of E_g modes for $\text{Ba}_2\text{LiOsO}_6$ and $\text{Ba}_2\text{NaOsO}_6$ from the all-phonon contribution is summarized in Table. V. These parameters can also be obtained based on the IFC from first-principles phonon calculations. However, as demonstrated in the Sec. III B, the $2 \times 2 \times 2$ q-mesh is used for the phonon calculations, meaning that only IFCs on a grid of $2 \times 2 \times 2$ can be generated. While the JT centers usually involves in atoms in more than one unit cell, the direct calculation of K matrix from IFC limits the analysis of the distance-dependence of elastic coupling. A full list of K_g matrix of E_g modes for different unit cells is shown in Table. S4 in the supporting information. On the other hand, for the contribution of uniform strain, VI.

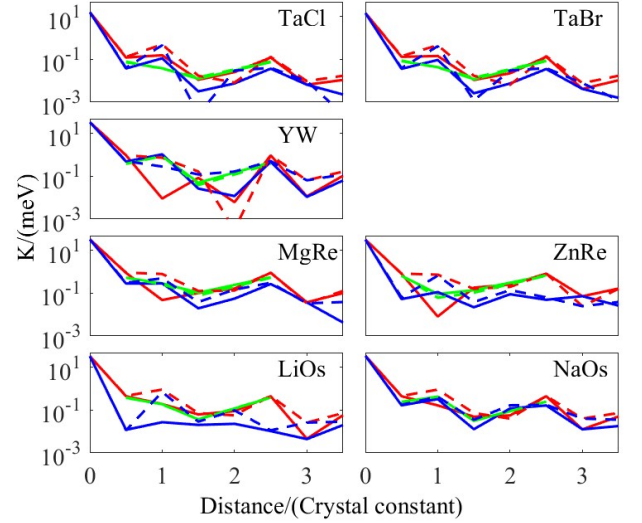


FIG. 3. Distance dependence of K based on all phonons. Red, green and blue represent the parameter $K_{E(\theta)}^{E(\theta)}(\mathbf{n})$, $K_{E(\theta)}^{E(\epsilon)}(\mathbf{n})$ and $K_{E(\epsilon)}^{E(\epsilon)}(\mathbf{n})$, respectively. The solid and dashed lines represents the process of calculating K matrix with and without the influence of periodicity.

IV. DISCUSSION

In order to have a straightforward comparison with other interaction strength, the elastic coupling matrix K is converted with respect to dimensionless JT active modes via $K/\sqrt{(\omega_{\Gamma\gamma}\omega_{\Gamma'\gamma'})M_{\Gamma\gamma}^{am}M_{\Gamma'\gamma'}^{am}}$, where M^{am} and $\omega_{\Gamma\gamma}$ are the mass of the corresponding atoms in JT mode $\Gamma\gamma$, and the vibration frequencies of $\Gamma\gamma$ JT active modes calculated by the K matrix, as shown in Table. VII. As discussed above, the Ξ matrix has $(\mathbf{n} - \mathbf{n}')^{-3}$ decay with respect to the distance between JT centers, which should be the same situation for elastic matrix K . The distance dependence of elastic coupling parameters ($K_{\mathbf{n}\Gamma\gamma'}^{\mathbf{n}'\Gamma\gamma}$) in Fig. 3 (solid line). This is the effective K matrix elements including the influence of surrounding JT centers in the crystals. On the other hand, in the extreme situation where there is only one JT impurity or there are only two JT impurities. The interactions between the two JT impurities and the JT active modes on the only one JT impurity become simpler, of which the procedure is shown in D, different from that described in II A 1. The results of such JT impurities with respect to distances are shown in Fig. 3 (dashed line).

For all the elastic matrix, from phonons or uniform strain, the onsite parameters have the degeneracy of 2, corresponding to the E_g JT active modes. To evaluate the dynamic situation, we calculate the contribution of the inter site JT energy and compared to the previous study[52], which is carried out with quantum chemistry computations, as shown in Table. VIII. E_{JT}^E is the amplitude of the JT stabilization of inter site case on the

TABLE V. Contribution from uniform strainThe distance dependent $K_{\mu'\gamma}^{\mu\gamma}(\mathbf{R})$ matrix in real space.The matrix correspondd to $\begin{pmatrix} K_{E_{g\theta}}^{E_{g\theta}} & K_{E_{g\theta}}^{E_{g\epsilon}} \\ K_{E_{g\epsilon}}^{E_{g\theta}} & K_{E_{g\epsilon}}^{E_{g\epsilon}} \end{pmatrix}$. R is the crystal constant. LGF, 2body, 1body and 1body(IFC) represent the data calculated with the method proposed in this paper, two-body coupling impurity, and one-body coupling, and calculated directly with interatomic force constants from first-principles calculations, respectively. The unit is meV.

		$0R$	$\sqrt{2}/2R$	$1R$	$\sqrt{6}/2R$	$2\sqrt{2}/2R$	$\sqrt{10}/2R$
NaOs	LGFs	$\begin{pmatrix} 71.176 & 0.000 \\ 0.000 & 71.176 \end{pmatrix}$	$\begin{pmatrix} -0.903 & -0.487 \\ -0.487 & -0.340 \end{pmatrix}$	$\begin{pmatrix} -0.338 & -0.866 \\ -0.866 & 0.662 \end{pmatrix}$	$\begin{pmatrix} -0.099 & -0.064 \\ -0.064 & -0.026 \end{pmatrix}$	$\begin{pmatrix} 0.114 & 0.000 \\ 0.000 & -0.241 \end{pmatrix}$	$\begin{pmatrix} -0.902 & 0.505 \\ 0.492 & -0.334 \end{pmatrix}$
	2body	$\begin{pmatrix} 71.358 & 0.009 \\ 0.009 & 71.347 \end{pmatrix}$	$\begin{pmatrix} -0.932 & -0.496 \\ -0.496 & -0.360 \end{pmatrix}$	$\begin{pmatrix} -1.844 & -0.858 \\ -0.858 & -0.853 \end{pmatrix}$	$\begin{pmatrix} -0.148 & -0.066 \\ -0.066 & -0.072 \end{pmatrix}$	$\begin{pmatrix} 0.081 & -0.000 \\ 0.000 & -0.341 \end{pmatrix}$	$\begin{pmatrix} -0.932 & 0.496 \\ 0.496 & -0.360 \end{pmatrix}$
	1body	$\begin{pmatrix} 71.342 & 0.000 \\ 0.000 & 71.342 \end{pmatrix}$	-	-	-	-	-
	1body (IFC)	$\begin{pmatrix} 75.840 & 0.000 \\ 0.000 & 75.840 \end{pmatrix}$	$\begin{pmatrix} -1.059 & -1.040 \\ -1.040 & 0.143 \end{pmatrix}$	-	-	-	-
LiOs	LGFs	$\begin{pmatrix} 68.005 & 0.000 \\ 0.000 & 68.005 \end{pmatrix}$	$\begin{pmatrix} -0.901 & -0.759 \\ -0.759 & -0.024 \end{pmatrix}$	$\begin{pmatrix} -0.388 & -0.384 \\ -0.384 & 0.055 \end{pmatrix}$	$\begin{pmatrix} -0.126 & -0.074 \\ -0.074 & -0.041 \end{pmatrix}$	$\begin{pmatrix} 0.183 & -0.000 \\ -0.000 & -0.046 \end{pmatrix}$	$\begin{pmatrix} -0.907 & 0.780 \\ 0.755 & -0.021 \end{pmatrix}$
	2body	$\begin{pmatrix} 68.185 & 0.011 \\ 0.011 & 68.172 \end{pmatrix}$	$\begin{pmatrix} -0.937 & -0.791 \\ -0.791 & -0.023 \end{pmatrix}$	$\begin{pmatrix} -1.858 & -0.370 \\ -0.370 & -1.431 \end{pmatrix}$	$\begin{pmatrix} -0.146 & -0.076 \\ -0.076 & -0.058 \end{pmatrix}$	$\begin{pmatrix} 0.115 & -0.000 \\ 0.000 & -0.197 \end{pmatrix}$	$\begin{pmatrix} -0.937 & 0.791 \\ 0.791 & -0.023 \end{pmatrix}$
	1body	$\begin{pmatrix} 68.164 & 0.000 \\ 0.000 & 68.164 \end{pmatrix}$	-	-	-	-	-
	1body (IFC)	$\begin{pmatrix} 71.103 & 0.000 \\ -0.000 & 71.103 \end{pmatrix}$	$\begin{pmatrix} -1.366 & -1.249 \\ -1.249 & 0.077 \end{pmatrix}$	-	-	-	-

TABLE VI. Contribution from uniform strain: $K_{\mu'\gamma}^{\mu\gamma}$ matrix in real space. The each 2×2 block correspondd to $\begin{pmatrix} K_{E_{g\theta}}^{E_{g\theta}} & K_{E_{g\theta}}^{E_{g\epsilon}} \\ K_{E_{g\epsilon}}^{E_{g\theta}} & K_{E_{g\epsilon}}^{E_{g\epsilon}} \end{pmatrix}$ of one JT center. The unit is meV.

	onsite							
NaOs	-14.040	0.000	-0.438	4.712	-0.438	-4.712	-8.599	-0.000
	0.000	-14.040	4.712	-5.878	-4.712	-5.878	-0.000	2.283
	-0.438	4.712	-2.061	2.927	1.102	1.019	0.664	-0.766
	4.712	-5.878	2.927	-5.441	-1.019	0.518	1.271	0.956
	-0.438	-4.712	1.102	-1.019	-2.061	-2.927	0.664	0.766
	-4.712	-5.878	1.019	0.518	-2.927	-5.441	-1.271	0.956
	-8.599	-0.000	0.664	1.271	0.664	-1.271	-7.131	0.000
	-0.000	2.283	-0.766	0.956	0.766	0.956	0.000	-0.371
LiOs	-15.532	0.000	-0.296	5.283	-0.283	-5.283	-9.481	-0.001
	-0.000	-15.532	5.285	-6.399	-5.302	-6.414	0.002	2.781
	-0.285	5.309	-2.184	2.928	1.437	1.452	0.567	-0.951
	5.311	-6.415	2.928	-5.565	-1.452	0.272	1.959	1.149
	-0.298	-5.292	1.421	-1.432	-2.184	-2.933	0.563	0.947
	-5.311	-6.399	1.431	0.287	-2.923	-5.565	-1.957	1.146
	-9.449	-0.002	0.567	1.920	0.571	-1.923	-7.255	0.000
	0.001	2.754	-0.937	1.134	0.940	1.138	-0.000	-0.493

trough is about 80 times larger than that of inter site case, which indicates unquenched dynamic JTE onsite in these systems.

The E_g JT modes frequencies of Ba_2MgWO_6 are about 540 cm^{-1} based on the Raman spectra [53], which should have similar value as Ba_2MgWO_6 . Our prediction for E_g JT modes frequencies of Ba_2MgWO_6 is 543.886 cm^{-1} , which appears close to that from experiment.

TABLE VII. The vibration frequency (cm^{-1}) of E_g JT active modes, calculated by the diagonalizing of the K matrix. ‘LiOs’, ‘NaOs’, ‘MgRe’, ‘ZnRe’, ‘YW’, ‘TaCl’, and ‘TaBr’ represent for $\text{Ba}_2\text{NaOsO}_6$, $\text{Ba}_2\text{LiOsO}_6$, $\text{Ba}_2\text{MgReO}_6$, $\text{Ba}_2\text{ZnReO}_6$, Cs_2TaCl_6 , Cs_2TaBr_6 , and Ba_2YWO_6 . LGF, 2body, 1body and 1body(IFC) represent the data calculated with the method proposed in this paper, two-body coupling impurity, and one-body coupling and calculated directly with interatomic force constants from first-principles calculations, respectively.

	LGF	2body	1body	1body(IFC)
NaOs	577.523	575.412	575.412	611.687
LiOs	551.796	549.781	549.792	573.481
MgRe	543.886	541.710	541.710	577.305
ZnRe	526.965	524.773	524.799	563.498
TaCl	266.012	264.996	264.996	268.737
TaBr	243.006	242.074	242.074	245.852
YW	560.837	557.397	557.418	604.508

TABLE VIII. The elastic energy between nearest JT centers.

	$\text{Ba}_2\text{NaOsO}_6$	$\text{Ba}_2\text{LiOsO}_6$
$q_{E\gamma}^{\mathbf{n}(0)}$ (a.u.)	10.24	12.29
E_{JT}^E (meV)	20.31	32.22
$K_{\mathbf{n}'}^{\mathbf{n}}(q_{E\gamma}^{\mathbf{n}(0)})^2$ (meV) :	$\begin{pmatrix} \theta\theta & \theta\epsilon \\ \epsilon\theta & \epsilon\epsilon \end{pmatrix}$	$\begin{pmatrix} 0.52 & 0.28 \\ 0.28 & 0.19 \end{pmatrix}$
		$\begin{pmatrix} 0.85 & 0.72 \\ 0.72 & 0.02 \end{pmatrix}$

V. CONCLUSIONS

In this paper, an effective Hamiltonian for a static cooperative JT effect is proposed, of which the all the necessary microscopic parameters can be obtained from first-principles calculations. This methodology is applied to a series of double perovskites $A_2B'BX_6$. This methodology can be, in general, used to investigate the APES of any type of the local distortions, such as impurities, defects, etc

ACKNOWLEDGEMENTS

Z.H. acknowledges the financial support of the research projects A-800079-00-00 and A-8000017-00-00 of the National University of Singapore. N.I. acknowledges the Grant-in-Aid for Scientific Research (Grant No. 22K03507) from the Japan Society for the Promotion of Science. The computational resources and services used in this work were provided by the VSC (Flemish Supercomputer Center) funded by the Research Foundation - Flanders (FWO) and the Flemish Government - department EWI.

Appendix A: Derivation of the effective elastic interaction matrix

Considering the following expression based on Eq. 3, and Eq. 2,

$$F_{\alpha_1\alpha_2\dots} = U_{\alpha_1\alpha_2\dots} + \sum_{\mathbf{n}} \sum_{\bar{\mu}\bar{\Gamma}\bar{\gamma}} \lambda_{\bar{\mu}\bar{\Gamma}\bar{\gamma}}^{\mathbf{n}} \left(q_{\bar{\mu}\bar{\Gamma}\bar{\gamma}}^{\mathbf{n}} - \sum_{\mu\Gamma\gamma} a_{\bar{\mu}\bar{\Gamma}\bar{\gamma}}^{\mathbf{n}}(\mu\Gamma\gamma) Q_{\mu\Gamma\gamma} \right) \quad (\text{A1})$$

with $\lambda_{\bar{\mu}\bar{\Gamma}\bar{\gamma}}^{\mathbf{n}}$ the Lagrange multipliers, the extrema equations are:

$$\frac{\partial F_{\alpha_1\alpha_2\dots}}{\partial Q_{\mu\Gamma\gamma}} = \omega_{\mu\Gamma} Q_{\mu\Gamma\gamma} - \sum_{\mathbf{n}} \sum_{\bar{\mu}\bar{\Gamma}\bar{\gamma}} \lambda_{\bar{\mu}\bar{\Gamma}\bar{\gamma}}^{\mathbf{n}} a_{\bar{\mu}\bar{\Gamma}\bar{\gamma}}^{\mathbf{n}}(\mu\Gamma\gamma) = 0 \quad (\text{A2})$$

$$\frac{\partial F_{\alpha_1\alpha_2\dots}}{\partial q_{\bar{\mu}\bar{\Gamma}\bar{\gamma}}^{\mathbf{n}}} = \frac{\partial \epsilon_{\alpha}^{\mathbf{n}}(\{q_{\bar{\mu}\bar{\Gamma}\bar{\gamma}}^{\mathbf{n}}\})}{\partial q_{\bar{\mu}\bar{\Gamma}\bar{\gamma}}^{\mathbf{n}}} + \lambda_{\bar{\mu}\bar{\Gamma}\bar{\gamma}}^{\mathbf{n}} = 0 \quad (\text{A3})$$

$$\frac{\partial F_{\alpha_1\alpha_2\dots}}{\partial \lambda_{\bar{\mu}\bar{\Gamma}\bar{\gamma}}^{\mathbf{n}}} = q_{\bar{\mu}\bar{\Gamma}\bar{\gamma}}^{\mathbf{n}} - \sum_{\mu\Gamma\gamma} a_{\bar{\mu}\bar{\Gamma}\bar{\gamma}}^{\mathbf{n}}(\mu\Gamma\gamma) Q_{\mu\Gamma\gamma} = 0. \quad (\text{A4})$$

With the Eq. A4, and multiplying $a_{\bar{\mu}\bar{\Gamma}\bar{\gamma}}^{\mathbf{n}}(\mu\Gamma\gamma)/\omega_{\Gamma\gamma}^2$ to Eq. A2, we have:

$$q_{\bar{\mu}\bar{\Gamma}\bar{\gamma}}^{\mathbf{n}} = \sum_{\mathbf{n}'\mu'\Gamma'\gamma'} \lambda_{\mathbf{n}'\mu'\Gamma'\gamma'}^{\mathbf{n}'} \Xi_{\mathbf{n}'\mu'\Gamma'\gamma'}^{\mathbf{n}\bar{\mu}\bar{\Gamma}\bar{\gamma}} \quad (\text{A5})$$

where $\Xi_{\mathbf{n}'\mu'\Gamma'\gamma'}^{\mathbf{n}\bar{\mu}\bar{\Gamma}\bar{\gamma}}$ is defined as:

$$\Xi_{\mathbf{n}'\mu'\Gamma'\gamma'}^{\mathbf{n}\bar{\mu}\bar{\Gamma}\bar{\gamma}} = \sum_{\mathbf{k}j} \frac{a_{\mu'\Gamma'\gamma'}^{\mathbf{n}'}(\mathbf{k}j) a_{\bar{\mu}\bar{\Gamma}\bar{\gamma}}^{\mathbf{n}}(\mathbf{k}j)}{\omega_{\mathbf{k}j}^2}. \quad (\text{A6})$$

Since the matrix Ξ consisting of the elastic parameters of the multi-atomic system only, is Hermitian, of which the inverse matrix ($K = \Xi^{-1}$) is Hermitian as well, the Lagrange multipliers can be expressed as

$$\lambda_{\bar{\mu}\bar{\Gamma}\bar{\gamma}}^{\mathbf{n}} = \sum_{\mathbf{n}'\mu'\Gamma'\gamma'} K_{\mathbf{n}'\mu'\Gamma'\gamma'}^{\mathbf{n}\bar{\mu}\bar{\Gamma}\bar{\gamma}} q_{\mu'\Gamma'\gamma'}^{\mathbf{n}'}. \quad (\text{A7})$$

The extrema expression based on only the local JT active modes can be obtained by substituting the expression Eq. A7 in to Eq. A3, which goes like:

$$\frac{\partial \epsilon_{\alpha}^{\mathbf{n}}(\{q_{\bar{\mu}\bar{\Gamma}\bar{\gamma}}^{\mathbf{n}}\})}{\partial q_{\bar{\mu}\bar{\Gamma}\bar{\gamma}}^{\mathbf{n}}} + \sum_{\mathbf{n}'\mu'\Gamma'\gamma'} K_{\mathbf{n}'\mu'\Gamma'\gamma'}^{\mathbf{n}\bar{\mu}\bar{\Gamma}\bar{\gamma}} q_{\mu'\Gamma'\gamma'}^{\mathbf{n}'} = 0 \quad (\text{A8})$$

Appendix B: Derivation of coefficients $a_{\mu\Gamma\gamma}^{\mathbf{n}}(\Gamma\gamma)$

The atomic displacements $u_{\kappa\alpha}(\mathbf{n})$ can be decomposed into the contributions from phonons ($u_{\kappa\alpha}^{ph}(\mathbf{n})$) and uniform strains ($u_{\kappa\alpha}^{us}(\mathbf{n})$), as

$$u_{\kappa\alpha}(\mathbf{n}) = u_{\kappa\alpha}^{ph}(\mathbf{n}) + u_{\kappa\alpha}^{us}(\mathbf{n}). \quad (\text{B1})$$

The uniform strain terms can be expressed as:

$$u_{\kappa\alpha}^{us}(\mathbf{n}) = \sum_{\beta} \tilde{\epsilon}_{\alpha\beta} R_{\alpha}(\mathbf{n}\kappa) \quad (\text{B2})$$

where $\mathbf{R}(\mathbf{n}\kappa)$ is the position of the atom ($\mathbf{n}\kappa$) in a common coordinate system and the coefficients $\tilde{\epsilon}_{\alpha\beta} = \partial u_{\alpha}^{us} / \partial R_{\beta}$ are constants in the case of uniform strains, of which the total number is nine. The nine coefficients includes 6 symmetric tensor elements, which are equivalent to the six tensor elements of the general strain, and 3 anti-symmetric tensor elements, describing the uniform bulk rotation of the crystal around three Cartesian axes. Thus, for the cooperative JT problem, the general strain tensor can be used as the coefficients $\tilde{\epsilon}_{\alpha\beta}$. Thus, Eq. B2, can be written as:

$$u_{\kappa\alpha}^{us}(\mathbf{n}) = \sum_{\beta} \epsilon_{\alpha\beta} R_{\alpha}(\mathbf{n}\kappa). \quad (\text{B3})$$

With the definition of JT active modes, Eq. 10, the uniform strains contribution, the second term in Eq. 23, becomes

$$q_{\mu\Gamma\gamma}^{\mathbf{n}} = \sum_{\alpha\beta} \left[\sum_{\mathbf{n}'\kappa\alpha} c_{\mu\Gamma\gamma}(\mathbf{n} - \mathbf{n}', \kappa, \alpha) R_{\beta}(\mathbf{n}', \kappa) \right] \epsilon_{\alpha\beta}. \quad (\text{B4})$$

The translational symmetry of the uniform strains results in the invariance of the coefficients $c_{\mu\Gamma\gamma}(\mathbf{n} - \mathbf{n}', \kappa, \alpha)$,

and $\sum_{\mathbf{n}'\kappa\alpha} c_{\mu\Gamma\gamma}(\mathbf{n} - \mathbf{n}', \kappa, \alpha) = 0$, which are valid for all the JT active modes. With the transformation between general strain and the symmetric strain, Eq. 21, we can obtain the expression of the coefficients for the uniform strain contribution, Eq. 24, in which the \mathbf{n} is omitted because of the translational invariance.

Appendix C: Derivation of the symmetrized elastic modulus for cubic systems

Starting from Eq. 18, for cubic system, there are only three independent elastic modulus element, of which the relations of all the element of elastic modulus is shown as following:

$$\begin{aligned}
C_{xxxx} &= C_{yyyy} = C_{zzzz} \\
C_{xxyy} &= C_{xxzz} = C_{yyzz} = C_{zzyy} = C_{zzxx} = C_{yyxx} \\
C_{xyxy} &= C_{yzyz} = C_{zxzx} \\
C_{xyzx} &= C_{xyxx} = C_{xyyy} = C_{xyzz} = C_{xyyz} = 0 \\
C_{yzxx} &= C_{yzyy} = C_{yzzz} = C_{xzxy} = C_{yzzx} = 0 \quad (C1) \\
C_{zxxx} &= C_{zxyy} = C_{zxzz} = C_{zxxxy} = C_{zxyyz} = 0 \\
C_{xxyy} &= C_{xxyy} = C_{xxzz} = C_{yyxy} = C_{yyyz} \\
&= C_{yyzx} = C_{zzxy} = C_{zzyz} = C_{zzzx} = 0
\end{aligned}$$

while $\varepsilon_{xy} = \varepsilon_{yx}$, $\varepsilon_{yz} = \varepsilon_{zy}$, and $\varepsilon_{zx} = \varepsilon_{xz}$, so that the Eq. 18 can be expanded as

$$\begin{aligned}
U_{us} &= \frac{NV_0}{2} C_{xxxx} (\varepsilon_{xx}^2 + \varepsilon_{yy}^2 + \varepsilon_{zz}^2) \\
&+ 2NV_0 C_{xxyy} (\varepsilon_{xy}^2 + \varepsilon_{yz}^2 + \varepsilon_{zx}^2) \\
&+ NV_0 C_{xyxy} (\varepsilon_{xx}\varepsilon_{yy} + \varepsilon_{xx}\varepsilon_{zz} + \varepsilon_{yy}\varepsilon_{zz}) \quad (C2)
\end{aligned}$$

The uniform strain is independent compared with the vibronic distortions for the static JT case. To study the contribution of uniform strain, we should express the contribution of uniform strain in the same basis set as the study of JT effect.

In the octahedral case, the symmetry should be O_h , where the Cartesian index, x, y, z, has the same symmetry of T_{1u} element. So the symmetrized basis set should be determined by the direct product $T_{1u} \otimes T_{1u} = A_1 \oplus E \oplus \{T_1\} \oplus T_2$. From the Koster's group tables, we have the relation between the symmetrized strains and the general strains, which are also the elements of Υ matrix defined in Eq. 21, as

$$\begin{aligned}
\varepsilon_{xx} &= \frac{1}{\sqrt{3}}\varepsilon_{A_1} - \frac{1}{\sqrt{6}}\varepsilon_{E(\theta)} + \frac{1}{\sqrt{2}}\varepsilon_{E(\epsilon)} \\
\varepsilon_{yy} &= \frac{1}{\sqrt{3}}\varepsilon_{A_1} - \frac{1}{\sqrt{6}}\varepsilon_{E(\theta)} - \frac{1}{\sqrt{2}}\varepsilon_{E(\epsilon)} \\
\varepsilon_{zz} &= \frac{1}{\sqrt{3}}\varepsilon_{A_1} + \frac{\sqrt{2}}{\sqrt{3}}\varepsilon_{E(\theta)} \quad (C3) \\
\varepsilon_{yz} &= \varepsilon_{T_2(\xi)} \\
\varepsilon_{zx} &= \varepsilon_{T_2(\eta)} \\
\varepsilon_{xy} &= \varepsilon_{T_2(\zeta)}
\end{aligned}$$

Substituting Eq. C3 into Eq. C2, we have

$$\begin{aligned}
U_{us} &= \frac{NV_0}{2} [(C_{xxxx} + 2C_{xxyy}) e_{A_1}^2 \\
&+ (C_{xxxx} - C_{xxyy}) e_{E(\theta)}^2 + (C_{xxxx} - C_{xxyy}) e_{E(\epsilon)}^2 \\
&+ 4C_{xyxy} (\varepsilon_{T_2(\xi)}^2 + \varepsilon_{T_2(\eta)}^2 + \varepsilon_{T_2(\zeta)}^2)] \quad (C4)
\end{aligned}$$

Comparing with the form in Eq. 20, we have the correspondence of general elastic modulus and the symmetrized elastic modulus as

$$\begin{aligned}
C_{A_1} &= C_{xxxx} + 2C_{xxyy} \\
C_{E(\theta)} &= C_{E(\epsilon)} = C_{xxxx} - C_{xxyy} \quad (C5) \\
C_{T_2(\xi)} &= C_{T_2(\eta)} = C_{T_2(\zeta)} = 4C_{xyxy}
\end{aligned}$$

Appendix D: K matrix for isolated JT impurities

This is to check the trend of K matrix elements with respect to the distance between two JT centers, for which there are three situations: 1). only considering the isolated one JT center, 2). considering JT pairs separated with a distance \mathbf{n} . The following derivations and calculations were done with the example of $\text{Ba}_2\text{NaOsO}_6$. In order to have a better comparison of the strength of elastic interactions, K matrix is transformed based on the dimensionless JT modes: $K^{dl} = K/(\omega \times M_{am})$.

1. Case 1: 1body JT center

In this situation, JT centers are treated as impurities, which means, there are only the two JT centers in the crystals. Thus, the K matrix will be calculated directly from Ξ matrix.

For on-site situation, the Ξ matrix considered should be a 2×2 matrix as

$$\Xi_{1body} = \begin{pmatrix} \Xi_{1E_\theta}^{1E_\theta} & \Xi_{1E_\theta}^{1E_\epsilon} \\ \Xi_{1E_\theta}^{1E_\epsilon} & \Xi_{1E_\epsilon}^{1E_\epsilon} \end{pmatrix} \quad (D1)$$

where, due to symmetry, $\Xi_{1E_\theta}^{1E_\theta} = \Xi_{1E_\epsilon}^{1E_\epsilon} = \Xi_0$, $\Xi_{1E_\theta}^{1E_\epsilon} = \Xi_{1E_\epsilon}^{1E_\theta} = 0$.

The corresponding K_{1body} matrix is determined by directly inverse the Ξ_{1body} matrix,

$$K_{1body} = \begin{pmatrix} K_{1E_\theta}^{1E_\theta} & K_{1E_\theta}^{1E_\epsilon} \\ K_{1E_\theta}^{1E_\epsilon} & K_{1E_\epsilon}^{1E_\epsilon} \end{pmatrix} = \begin{pmatrix} \frac{1}{\Xi_0} & 0 \\ 0 & \frac{1}{\Xi_0} \end{pmatrix} \quad (D2)$$

and the corresponding frequencies $\omega_{1body} = \sqrt{1/(\Xi_0 * M^{am})}$.

2. Case 2: JT interacting pairs

For the interactions involving two JT centers, the Ξ matrix should be a 4×4 matrix, consisting of two 2×2 matrices corresponding to 2 JT centers, as

$$\Xi_{2body}(\mathbf{R}) = \begin{pmatrix} \Xi_{1E_\theta}^{1E_\theta} & \Xi_{1E_\epsilon}^{1E_\theta} & \Xi_{2E_\theta}^{1E_\theta}(\mathbf{R}) & \Xi_{2E_\epsilon}^{1E_\theta}(\mathbf{R}) \\ \Xi_{1E_\theta}^{1E_\epsilon} & \Xi_{1E_\epsilon}^{1E_\epsilon} & \Xi_{2E_\theta}^{1E_\epsilon}(\mathbf{R}) & \Xi_{2E_\epsilon}^{1E_\epsilon}(\mathbf{R}) \\ \Xi_{1E_\theta}^{2E_\theta}(\mathbf{R}) & \Xi_{1E_\epsilon}^{2E_\theta}(\mathbf{R}) & \Xi_{2E_\theta}^{2E_\theta} & \Xi_{2E_\epsilon}^{2E_\theta} \\ \Xi_{1E_\theta}^{2E_\epsilon}(\mathbf{R}) & \Xi_{1E_\epsilon}^{2E_\epsilon}(\mathbf{R}) & \Xi_{2E_\theta}^{2E_\epsilon} & \Xi_{2E_\epsilon}^{2E_\epsilon} \end{pmatrix} \quad (D3)$$

$$= \begin{pmatrix} \Xi_{1E_\theta}^{1E_\theta} & 0 & \Xi_{2E_\theta}^{1E_\theta}(\mathbf{R}) & \Xi_{2E_\epsilon}^{1E_\theta}(\mathbf{R}) \\ 0 & \Xi_{1E_\epsilon}^{1E_\epsilon} & \Xi_{2E_\theta}^{1E_\epsilon}(\mathbf{R}) & \Xi_{2E_\epsilon}^{1E_\epsilon}(\mathbf{R}) \\ \Xi_{1E_\theta}^{2E_\theta}(\mathbf{R}) & \Xi_{1E_\epsilon}^{2E_\theta}(\mathbf{R}) & \Xi_{2E_\theta}^{2E_\theta} & 0 \\ \Xi_{1E_\theta}^{2E_\epsilon}(\mathbf{R}) & \Xi_{1E_\epsilon}^{2E_\epsilon}(\mathbf{R}) & 0 & \Xi_{2E_\epsilon}^{2E_\epsilon} \end{pmatrix} \quad (D4)$$

, where $\mathbf{R} = \mathbf{n} - \mathbf{n}'$ is the vector between the two JT centers locating in \mathbf{n} , and \mathbf{n}' , respectively.

The corresponding $K_{2body}(\mathbf{R})$ matrix is determined by the direct inverse of $\Xi_{2body}(\mathbf{R})$:

$$K_{2body}(\mathbf{R}) = inv \begin{pmatrix} \Xi_{1E_\theta}^{1E_\theta} & 0 & \Xi_{2E_\theta}^{1E_\theta}(\mathbf{R}) & \Xi_{2E_\epsilon}^{1E_\theta}(\mathbf{R}) \\ 0 & \Xi_{1E_\epsilon}^{1E_\epsilon} & \Xi_{2E_\theta}^{1E_\epsilon}(\mathbf{R}) & \Xi_{2E_\epsilon}^{1E_\epsilon}(\mathbf{R}) \\ \Xi_{1E_\theta}^{2E_\theta}(\mathbf{R}) & \Xi_{1E_\epsilon}^{2E_\theta}(\mathbf{R}) & \Xi_{2E_\theta}^{2E_\theta} & 0 \\ \Xi_{1E_\theta}^{2E_\epsilon}(\mathbf{R}) & \Xi_{1E_\epsilon}^{2E_\epsilon}(\mathbf{R}) & 0 & \Xi_{2E_\epsilon}^{2E_\epsilon} \end{pmatrix} \quad (D5)$$

$$= \begin{pmatrix} K_{1E_\theta}^{1E_\theta} & K_{1E_\epsilon}^{1E_\theta} & K_{2E_\theta}^{1E_\theta}(\mathbf{R}) & K_{2E_\epsilon}^{1E_\theta}(\mathbf{R}) \\ K_{1E_\theta}^{1E_\epsilon} & K_{1E_\epsilon}^{1E_\epsilon} & K_{2E_\theta}^{1E_\epsilon}(\mathbf{R}) & K_{2E_\epsilon}^{1E_\epsilon}(\mathbf{R}) \\ K_{1E_\theta}^{2E_\theta}(\mathbf{R}) & K_{1E_\epsilon}^{2E_\theta}(\mathbf{R}) & K_{2E_\theta}^{2E_\theta} & K_{2E_\epsilon}^{2E_\theta} \\ K_{1E_\theta}^{2E_\epsilon}(\mathbf{R}) & K_{1E_\epsilon}^{2E_\epsilon}(\mathbf{R}) & K_{2E_\theta}^{2E_\epsilon} & K_{2E_\epsilon}^{2E_\epsilon} \end{pmatrix} \quad (D6)$$

Since the 2×2 block of the onsite interaction might not be diagonal, a diagonalization procedure is required, from which the frequencies are determined from the $K_{1E_\theta}^{1E_\theta}(\mathbf{R} = \mathbf{0}, diag)$: $\omega_{crystal} = \sqrt{K_{1E_\theta}^{1E_\theta}(\mathbf{R} = \mathbf{0}, diag)/M^{am}}$.

-
- [1] Yu. E. Perlin and Max Wagner, “The dynamical jahn-teller effect in localized systems,” (1984).
- [2] R. D. Willett, D. Gatteschi, and O. Kahn, *Magneto-structural correlations in exchange coupled systems* (D Reidel Publishing Co, United States, 1985).
- [3] T. Riste, *Electron-phonon Interactions and Phase Transitions*, NATO ASI series. Series B: Physics (Plenum Press, 1977).
- [4] Isaac B. Bersuker and Victor Z. Polinger, “Vibronic interactions in molecules and crystals,” (1989).
- [5] G. A. Gehring and K. A. Gehring, “Co-operative jahn-teller effects,” *Reports on Progress in Physics* **38**, 1 (1975).
- [6] Michael D Kaplan and Benjamin G Vekhter, *Cooperative Phenomena in Jahn–Teller Crystals* (Springer Science & Business Media, 2012).
- [7] L. F. Chibotaru, “One-centre-coordinate approach to the investigation of the jahn–teller effect in two-centre vibronic systems with common atoms,” *Chemical Physics Letters* **195**, 109–114 (1992).
- [8] L. F. Chibotaru, “Adiabatic potential of the system of two equivalent vibronic centres with common atoms i. one-centre-coordinate approach,” *Molecular Physics* **81**, 873–889 (1994), doi: 10.1080/00268979400100591.
- [9] G. I. Bersuker, L. F. Chibotaru, V. Z. Polinger, and A. O. Solonenko, “Effects of vibrational intercentre interaction in a trigonal two-centre system with twofold electronic degeneracy at each centre,” *Molecular Physics* **70**, 1031–1043 (1990).
- [10] Pavel Novák, “Interactions between octahedrally coordinated eg jahn-teller ions,” *Journal of Physics and Chemistry of Solids* **30**, 2357–2364 (1969).
- [11] Pavel Novák, “Some aspects of the cooperative jahn-teller effect in spinel and perovskite systems,” *Journal of Physics and Chemistry of Solids* **31**, 125–130 (1970).
- [12] William Witczak-Krempa, Gang Chen, Yong Baek Kim, and Leon Balents, “Correlated quantum phenomena in the strong spin-orbit regime,” *Annual Review of Condensed Matter Physics* **5**, 57–82 (2014).
- [13] Sami Vasala and Maarit Karppinen, “A2b’b’o6 perovskites: A review,” *Progress in Solid State Chemistry* **43**, 1–36 (2015).
- [14] C. M. Thompson, J. P. Carlo, R. Flacau, T. Aharen, I. A. Leahy, J. R. Pollichiemi, T. J. S. Munsie, T. Medina, G. M. Luke, J. Munevar, S. Cheung, T. Goko, Y. J. Uemura, and J. E. Greedan, “Long-range magnetic order in the 5d(2) double perovskite ba2caoso6: comparison with spin-disordered ba2yreo6,” *Journal of Physics-Condensed Matter* **26** (2014), 10.1088/0953-8984/26/30/306003, thompson, C. M. Carlo, J. P. Flacau, R. Aharen, T. Leahy, I. A. Pollichiemi, J. R. Munsie, T. J. S. Medina, T. Luke, G. M. Munevar, J. Cheung, S. Goko, T. Uemura, Y. J. Greedan, J. E. Luke, Graeme/A-9094-2010 Luke, Graeme/0000-0003-4762-1173; Leahy, Ian/0000-0002-4483-1813; Carlo, Jeremy/0000-0002-3925-5938 1361-648x.
- [15] C. M. Thompson, C. A. Marjerrison, A. Z. Sharma, C. R. Wiebe, D. D. Maharaj, G. Sala, R. Flacau, A. M. Hallas, Y. Cai, B. D. Gaulin, G. M. Luke, and J. E. Greedan, “Frustrated magnetism in the double perovskite la2liroo6: A comparison with la2liruo6,” *Physical Review B* **93** (2016), 10.1103/PhysRevB.93.014431, thompson, C. M. Marjerrison, C. A. Sharma, A. Z. Wiebe, C. R. Maharaj, D. D. Sala, G. Flacau, R. Hallas, A. M. Cai, Y. Gaulin, B. D. Luke, G. M. Greedan, J. E. Sala, Gabriele/W-2778-2018; Luke, Graeme/A-9094-2010; Wiebe, Christopher/Q-6085-2017; Gaulin, Bruce/AAP-6799-2021; Hallas,

- Alannah/AAZ-5286-2021 Sala, Gabriele/0000-0002-6654-0275; Luke, Graeme/0000-0003-4762-1173; Wiebe, Christopher/0000-0002-3681-0182; 2469-9969.
- [16] Y. H. Yuan, H. L. Feng, M. P. Ghimire, Y. Matsushita, Y. Tsujimoto, J. F. He, M. Tanaka, Y. Katsuya, and K. Yamaura, "High-pressure synthesis, crystal structures, and magnetic properties of 5d double-perovskite oxides $\text{Ca}_2\text{MgOsO}_6$ and $\text{Sr}_2\text{MgOsO}_6$," *Inorganic Chemistry* **54**, 3422–3431 (2015), yuan, Yahua Feng, Hai L. Ghimire, Madhav Prasad Matsushita, Yoshitaka Tsujimoto, Yoshihiro He, Jianfeng Tanaka, Masahiko Katsuya, Yoshio Yamaura, Kazunari MATSUSHITA, Yoshitaka/H-2734-2011; KATSUYA, Yoshio/B-9536-2013; Feng, Hai L/J-4189-2013; Ghimire, Madhav Prasad/AAH-5829-2019; Tsujimoto, Yoshihiro/H-6034-2012; YAMAURA, KAZUNARI/AEW-0565-2022; Ghimire, Madhav Prasad/AAT-3026-2021 MATSUSHITA, Yoshitaka/0000-0002-4968-8905; KATSUYA, Yoshio/0000-0001-5710-7448; Feng, Hai L/0000-0002-2699-3958; Tsujimoto, Yoshihiro/0000-0003-2140-3362; YAMAURA, KAZUNARI/0000-0003-0390-8244; Ghimire, Madhav Prasad/0000-0003-2783-4008 1520-510x.
- [17] Dan Liu, Naoya Iwahara, and Liviu F. Chibotaru, "Dynamical jahn-teller effect of fullerene anions," *Physical Review B* **97** (2018), 10.1103/PhysRevB.97.115412.
- [18] Dan Liu, Yasuyuki Niwa, Naoya Iwahara, Tohru Sato, and Liviu F. Chibotaru, "Quadratic jahn-teller effect of fullerene anions," *Physical Review B* **98** (2018), 10.1103/PhysRevB.98.035402.
- [19] Zhishuo Huang and Dan Liu, "Dynamical jahn-teller effect in the first excited c_{60}^- ," *International Journal of Quantum Chemistry* **120**, e26148 (2020).
- [20] R. Englman, *The Jahn-Teller effect in molecules and crystals* (Wiley-Interscience, London;New York;, 1972).
- [21] J. H. Van Vleck, "Paramagnetic relaxation times for titanium and chrome alum," *Physical Review* **57**, 426–447 (1940), van Vleck, JH.
- [22] Granino Arthur Korn and Theresa M Korn, *Mathematical handbook for scientists and engineers: definitions, theorems, and formulas for reference and review* (Courier Corporation, 2000).
- [23] A. A. Maradudin, E. W. Montroll, and George Herbert Weiss, *Theory of lattice dynamics in the harmonic approximation*, Vol. 3 (Academic Press, New York, 1963).
- [24] Richard M. Martin, *Electronic Structure: Basic Theory and Practical Methods* (Cambridge University Press, Cambridge, 2004).
- [25] Zhishuo Huang, Munirah D. Albaqami, Tohru Sato, Naoya Iwahara, and Liviu F. Chibotaru, "Jahn-teller effect in the cubic fullerides A_3C_{60} ," *Physical Review B* **103** (2021), 10.1103/PhysRevB.103.134102.
- [26] P. A. Flinn and A. A. Maradudin, "Distortion of crystals by point defects," *Annals of Physics* **18**, 81–109 (1962).
- [27] Stefano Baroni, Stefano de Gironcoli, Andrea Dal Corso, and Paolo Giannozzi, "Phonons and related crystal properties from density-functional perturbation theory," *Reviews of Modern Physics* **73**, 515–562 (2001), rMP.
- [28] Atsushi Togo, Laurent Chaput, Terumasa Tadano, and Isao Tanaka, "Implementation strategies in phonopy and phono3py," *Journal of Physics: Condensed Matter* **35**, 353001 (2023).
- [29] R. L. Melcher, "1 - the anomalous elastic properties of materials undergoing cooperative jahn-teller phase transitions," in *Physical Acoustics*, Vol. 12, edited by Warren P. Mason and R. N. Thurston (Academic Press, 1976) pp. 1–77.
- [30] Max Born and Kun Huang, *Dynamical theory of crystal lattices* (Clarendon Press, Oxford, England, 1954) pp. 229–236.
- [31] L. D. Landau and E. M. Lifshitz, *Theory of elasticity*, Vol. 7 (Pergamon Press, Reading, Mass;London;, 1959) qA931 Lan.
- [32] J. Kanamori, "Crstal distortion in magnetic compounds," *Journal of Applied Physics* **31**, S14–S23 (1960), kanamori, j.
- [33] Katharine E. Stitzer, Mark D. Smith, and Hans-Conrad zur Loye, "Crystal growth of $\text{Ba}_2\text{MgOsO}_6$ ($m=\text{li, na}$) from reactive hydroxide fluxes," *Solid State Sciences* **4**, 311–316 (2002).
- [34] C. A. Marjerrison, C. M. Thompson, G. Sala, D. D. Maharaj, E. Kermarrec, Y. Cai, A. M. Hallas, M. N. Wilson, T. J. S. Munsie, G. E. Granroth, R. Flacau, J. E. Greedan, B. D. Gaulin, and G. M. Luke, "Cubic $\text{re}(6+)$ ($5d(1)$) double perovskites, $\text{Ba}_2(\text{MgReO})_6$, $\text{Ba}_2(\text{ZnReO})_6$, and $\text{Ba}_2(\text{Y}(2/3)\text{ReO})_6$: Magnetism, heat capacity, μSR , and neutron scattering studies and comparison with theory," *Inorg Chem* **55**, 10701–10713 (2016), marjerrison, Casey A Thompson, Corey M Sala, Gabrielle Maharaj, Dalini D Kermarrec, Edwin Cai, Yipeng Hallas, Alannah M Wilson, Murray N Munsie, Timothy J S Granroth, Garrett E Flacau, Roxana Greedan, John E Gaulin, Bruce D Luke, Graeme M eng 2016/10/05 Inorg Chem. 2016 Oct 17;55(20):10701-10713. doi: 10.1021/acs.inorgchem.6b01933. Epub 2016 Oct 4.
- [35] Victor da Cruz Pinha Barbosa, Jie Xiong, Phuong Minh Tran, Michael A. McGuire, Jiaqiang Yan, Matthew T. Warren, Rolando Valdes Aguilar, Wenjuan Zhang, Mohit Randeria, Nandini Trivedi, Daniel Haskel, and Patrick M. Woodward, "The impact of structural distortions on the magnetism of double perovskites containing 5d1 transition-metal ions," *Chemistry of Materials* **34**, 1098–1109 (2022).
- [36] S. Lee, Wonjun Lee, W. Guohua, J. Ma, H. Zhou, M. Lee, E. S. Choi, and K. Y. Choi, "Experimental evidence for a valence-bond glass in the 5d1 double perovskite Ba_2YWO_6 ," *Physical Review B* **103** (2021), 10.1103/PhysRevB.103.224430.
- [37] Hoseop Yun and Gyung-Joo Jang, "Dicaesium hexachlorotantalate(IV), Cs_2TaCl_6 ," *Acta Crystallographica Section E Structure Reports Online* **63**, i22–i23 (2006).
- [38] H. Ishikawa, T. Yajima, A. Matsuo, and K. Kindo, "Ligand dependent magnetism of the $\text{jeff}=3/2$ mott insulator $\text{Cs}_2\text{Mx}(6)$ ($m=\text{Ta, Nb, X}=\text{Br, Cl}$)," *J Phys Condens Matter* **33** (2021), 10.1088/1361-648X/abd7b5, ishikawa, Hajime Yajima, Takeshi Matsuo, Akira Kindo, Koichi eng England 2021/01/20 J Phys Condens Matter. 2021 Jan 18;33(12). doi: 10.1088/1361-648X/abd7b5.
- [39] G. Kresse and J. Furthmüller, "Efficiency of ab-initio total energy calculations for metals and semiconductors using a plane-wave basis set," *Computational Materials Science* **6**, 15–50 (1996).
- [40] G. Kresse and J. Furthmüller, "Efficient iterative schemes for ab initio total-energy calculations using a plane-wave basis set," *Physical Review B* **54**, 11169–11186 (1996).
- [41] G. Kresse and J. Hafner, "Ab initio molecular dynamics for liquid metals," *Physical Review B* **47**, 558–561 (1993).

- [42] G. Kresse and J. Hafner, “Ab initio molecular-dynamics simulation of the liquid-metal amorphous-semiconductor transition in germanium,” *Physical Review B* **49**, 14251–14269 (1994).
- [43] P. E. Blöchl, “Projector augmented-wave method,” *Physical Review B* **50**, 17953–17979 (1994).
- [44] G. Kresse and D. Joubert, “From ultrasoft pseudopotentials to the projector augmented-wave method,” *Physical Review B* **59**, 1758–1775 (1999).
- [45] John P. Perdew, Kieron Burke, and Matthias Ernzerhof, “Generalized gradient approximation made simple,” *Physical Review Letters* **77**, 3865–3868 (1996).
- [46] John P. Perdew, Kieron Burke, and Matthias Ernzerhof, “Generalized gradient approximation made simple [phys. rev. lett. 77, 3865 (1996)],” *Physical Review Letters* **78**, 1396–1396 (1997).
- [47] Atsushi Togo, “First-principles phonon calculations with phonopy and phono3py,” *J. Phys. Soc. Jpn.* **92**, 012001 (2023).
- [48] Atsushi Togo, Laurent Chaput, Terumasa Tadano, and Isao Tanaka, “Implementation strategies in phonopy and phono3py,” *J. Phys. Condens. Matter* **35**, 353001 (2023).
- [49] Yvon Le Page and Paul Saxe, “Symmetry-general least-squares extraction of elastic data for strained materials from ab initio calculations of stress,” *Physical Review B* **65** (2002), 10.1103/PhysRevB.65.104104.
- [50] Xifan Wu, David Vanderbilt, and D. R. Hamann, “Systematic treatment of displacements, strains, and electric fields in density-functional perturbation theory,” *Physical Review B* **72** (2005), 10.1103/PhysRevB.72.035105.
- [51] R. Orbach and M. Tachiki, “Phonon-induced ion-ion coupling in paramagnetic salts,” *Physical Review* **158**, 524–524 (1967), orbach, r tachiki, m.
- [52] Naoya Iwahara, Veacheslav Vieru, and Liviu F. Chibotaru, “Spin-orbital-lattice entangled states in cubic d^1 double perovskites,” *Physical Review B* **98** (2018), 10.1103/PhysRevB.98.075138.
- [53] Jana Pásztorová, Wen Hua Bi, Richard Gaal, Karl Krämer, Ivica Živković, and Henrik M. Røonnøw, “Structure, heat capacity and raman spectra of Ba_2MgWO_6 single crystals grown in $\text{BaCl}_2\text{-MgCl}_2$ flux,” *Journal of Solid State Chemistry* **326** (2023), 10.1016/j.jssc.2023.124184.

TABLE S1. $Fm\bar{3}m$ position correspondence of $A_2B'BX_6$, x should be provided to fully determine the structure.

P_label	atom_in	crystal position	P_label	atom_in	crystal position	atom_in	crystal position
A(8c)	1	(0.25, 0.25, 0.25)	X(24e)	17	(x,0.00,0.00)	29	(0.50+x,0.00,0.50)
	2	(0.75, 0.75, 0.75)		18	(1.00-x,0.00,0.00)	30	(0.50-x,0.00,0.50)
	3	(0.75, 0.75, 0.25)		19	(0.00,x,0.00)	31	(0.50,x,0.50)
	4	(0.25, 0.25, 0.75)		20	(0.00,1.00-x,0.00)	32	(0.50,1.00-x,0.50)
	5	(0.75, 0.25, 0.75)		21	(0.00,0.00,x)	33	(0.50,0.00,0.50+x)
	6	(0.25, 0.75, 0.25)		22	(0.00,0.00,1.00-x)	34	(0.50,0.00,0.50-x)
	7	(0.25, 0.75, 0.75)		23	(x,0.50,0.50)	35	(0.50+x,0.50,0.00)
	8	(0.75, 0.25, 0.25)		24	(1.00-x,0.50,0.50)	36	(0.50-x,0.50,0.00)
B'(4b)	9	(0.50,0.50,0.50)	25	(0.00,0.50+x,0.50)	37	(0.50,0.50+x,0.00)	
	10	(0.50,0.00,0.00)	26	(0.00,0.50-x,0.50)	38	(0.50,0.50-x,0.00)	
	11	(0.00,0.50,0.00)	27	(0.00,0.50,0.50+x)	39	(0.50,0.50,x)	
	12	(0.00,0.00,0.50)	28	(0.00,0.50,0.50-x)	40	(0.50,0.50,1.00-x)	
B(4a)	13	(0.00,0.00,0.00)					
	14	(0.00,0.50,0.50)					
	15	(0.50,0.00,0.50)					
	16	(0.50,0.50,0.00)					

Supplemental Materials: First-principles derivation of elastic interaction between Jahn-Teller centers in crystals via LGFs

Before showing the information in this document, one thing should be noted that for simplicity, ‘LiOs’, ‘NaOs’, ‘MgRe’, ‘ZnRe’, ‘YW’, ‘TaCl’, and ‘TaBr’ represent for Ba_2LiOsO_6 , Ba_2NaOsO_6 , Ba_2MgReO_6 , Ba_2ZnReO_6 , Ba_2YWO_6 , Cs_2TaCl_6 , and Cs_2TaBr_6 , respectively.

This document includes the following information:

The phonon dispersions of all the seven double perovskites studied in this paper are shown in Fig. S1.

The position order of atoms in the convention unit cell is shown in Table. S1.

The Ξ matrix from full phonons, for the inter site, the nearest, next nearest, next next nearest, next next next nearest, next next next next nearest sites, for all the double perovskites are shown in Table. S2. The Ξ matrix contributed from acoustic phonons, for the inter site, the nearest, next nearest, next next nearest, next next next nearest, next next next next nearest sites, for all the double perovskites are shown in Table. S2.

All the Ξ matrix from the uniform strain are shown in Table. S3.

The K matrix of only E_g JT active modes for the original, nearest, next nearest convention unit cells, from full phonons are shown in Table. S4.

The K matrix from the uniform strain is summarized in Table. S5.

The K matrix from IFCs are shown in Table. S6.

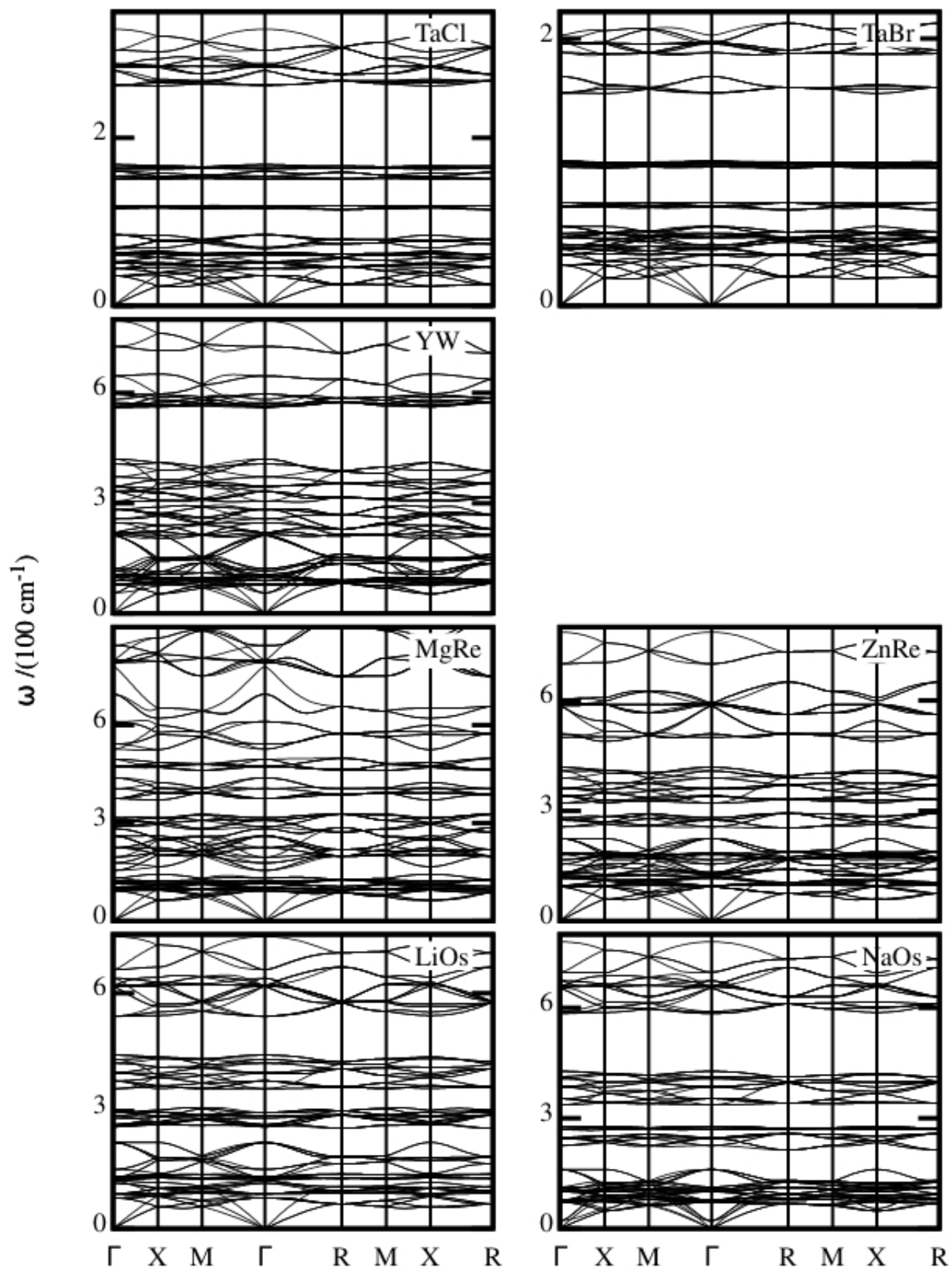


FIG. S1. Phonon dispersions of double perovskites.

TABLE S2. Ξ matrix for both intra and inter JT active centers. The inter site interaction is labeled as 1N, 2N, 3N, 4N, 5N, for the nearest, next nearest, next next nearest, next next next nearest, next next next next nearest sites, respectively. JTC1, JTC2, JTC3 are the label for the JT active centers, as defined in Table. II. From the left to right, and from the top to bottom, the matrix elements correspond to JTD_2, JTD_3, JTD_4, JTD_5 and JTD_6, respectively. The unit is $m_e\hbar\omega^2/Ry$.

	Intra			1N			2N			3N			4N			5N																
	(0,0,0) (JTC1,JTC1)			(0,0,0) (JTC1,JTC2)			(0,1,0) (JTC1,JTC1)			(0,1,0) (JTC1,JTC3)			(0,1,1) (JTC1,JTC1)			(0,1,0) (JTC1,JTC2)																
NaOs	4.988	0.000	0.000	0.000	0.000	0.000	0.065	0.035	-0.087	0.000	0.000	-0.060	0.000	0.000	0.000	0.010	-0.005	-0.008	-0.001	0.001	0.016	0.013	-0.010	0.000	0.000	0.001	-0.008	0.001	0.000	0.000		
LiOs	5.464	0.000	0.000	0.000	0.000	0.000	0.075	0.063	-0.051	0.000	0.000	-0.030	0.115	0.000	0.000	0.000	-0.006	0.005	-0.002	0.000	-0.010	0.011	-0.003	0.021	0.000	0.000	0.000	-0.003	-0.005	0.011	0.000	0.000
MgRe	5.628	0.000	0.000	0.000	0.000	0.000	0.090	0.052	0.172	0.000	0.000	-0.044	0.084	0.000	0.000	0.000	-0.013	0.007	-0.011	0.005	-0.021	0.021	-0.011	0.039	0.000	0.000	-0.009	-0.015	0.025	0.000	0.000	
ZnRe	5.997	0.000	0.000	0.000	0.000	0.000	0.124	0.012	0.166	0.000	0.000	-0.011	0.124	0.000	0.000	0.000	-0.020	0.007	-0.005	0.001	-0.023	0.030	-0.021	0.039	0.000	0.000	-0.005	-0.004	0.016	0.000	0.000	
TaCl	10.614	0.000	0.000	0.000	0.000	0.000	0.085	0.051	-0.085	0.000	0.000	0.326	-0.024	0.000	0.000	0.000	-0.009	0.000	-0.009	0.008	-0.019	0.011	0.001	0.025	0.000	0.000	-0.004	-0.009	0.017	0.000	0.000	
TaBr	12.719	0.000	0.000	0.000	0.000	0.000	0.120	0.075	-0.105	0.000	0.000	0.392	-0.035	0.000	0.000	0.000	-0.015	-0.012	-0.020	0.007	-0.001	0.018	0.013	-0.018	0.000	0.000	0.002	-0.006	-0.003	0.000	0.000	
YW	5.316	0.000	0.000	0.000	0.000	0.000	0.148	0.059	-0.085	0.000	0.000	0.115	-0.138	0.000	0.000	0.000	0.026	-0.006	-0.013	0.002	-0.006	0.019	0.011	-0.023	0.000	0.000	0.002	-0.016	0.013	0.000	0.000	

TABLE S3. Ξ matrix contributed from uniform strain for the four JT active centers in unconvention unit cell. JTC1, JTC2, JTC3 are the label for the JT active centers, as defined in Table. II. From the left to right, and from the top to bottom, the matrix elements correspond to JTD_2, JTD_3, JTD_4, JTD_5 and JTD_6, respectively. The unit is $bohr^2/Ry$.

	(0,0,0) (JTC1,JTC1)	(0,0,0) (JTC1,JTC2)
NaOs	$\begin{pmatrix} 0.267 & 0.000 & 0.000 & 0.000 & 0.000 \\ 0.000 & 0.267 & 0.000 & 0.000 & 0.000 \\ 0.000 & 0.000 & 0.313 & 0.000 & 0.000 \\ 0.000 & 0.000 & 0.000 & 0.313 & 0.000 \\ 0.000 & 0.000 & 0.000 & 0.000 & 0.313 \end{pmatrix}$	$\begin{pmatrix} 0.033 & -0.081 & 0.000 & 0.000 & 0.000 \\ -0.081 & 0.127 & 0.000 & 0.000 & 0.000 \\ 0.000 & 0.000 & -0.016 & 0.000 & 0.000 \\ 0.000 & 0.000 & 0.000 & 0.148 & 0.000 \\ 0.000 & 0.000 & 0.000 & 0.000 & 0.148 \end{pmatrix}$
LiOs	$\begin{pmatrix} 0.386 & 0.000 & 0.000 & 0.000 & 0.000 \\ 0.000 & 0.386 & 0.000 & 0.000 & 0.000 \\ 0.000 & 0.000 & 0.243 & 0.000 & 0.000 \\ 0.000 & 0.000 & 0.000 & 0.243 & 0.000 \\ 0.000 & 0.000 & 0.000 & 0.000 & 0.243 \end{pmatrix}$	$\begin{pmatrix} 0.047 & -0.117 & 0.000 & 0.000 & 0.000 \\ -0.117 & 0.182 & 0.000 & 0.000 & 0.000 \\ 0.000 & 0.000 & -0.013 & 0.000 & 0.000 \\ 0.000 & 0.000 & 0.000 & 0.115 & 0.000 \\ 0.000 & 0.000 & 0.000 & 0.000 & 0.115 \end{pmatrix}$
MgRe	$\begin{pmatrix} 0.217 & 0.000 & 0.000 & 0.000 & 0.000 \\ 0.000 & 0.217 & 0.000 & 0.000 & 0.000 \\ 0.000 & 0.000 & 0.170 & 0.000 & 0.000 \\ 0.000 & 0.000 & 0.000 & 0.170 & 0.000 \\ 0.000 & 0.000 & 0.000 & 0.000 & 0.170 \end{pmatrix}$	$\begin{pmatrix} 0.026 & -0.066 & 0.000 & 0.000 & 0.000 \\ -0.066 & 0.102 & 0.000 & 0.000 & 0.000 \\ 0.000 & 0.000 & -0.009 & 0.000 & 0.000 \\ 0.000 & 0.000 & 0.000 & 0.080 & 0.000 \\ 0.000 & 0.000 & 0.000 & 0.000 & 0.080 \end{pmatrix}$
ZnRe	$\begin{pmatrix} 0.321 & 0.000 & 0.000 & 0.000 & 0.000 \\ 0.000 & 0.321 & 0.000 & 0.000 & 0.000 \\ 0.000 & 0.000 & 0.210 & 0.000 & 0.000 \\ 0.000 & 0.000 & 0.000 & 0.210 & 0.000 \\ 0.000 & 0.000 & 0.000 & 0.000 & 0.210 \end{pmatrix}$	$\begin{pmatrix} 0.039 & -0.098 & 0.000 & 0.000 & 0.000 \\ -0.098 & 0.152 & 0.000 & 0.000 & 0.000 \\ 0.000 & 0.000 & -0.012 & 0.000 & 0.000 \\ 0.000 & 0.000 & 0.000 & 0.099 & 0.000 \\ 0.000 & 0.000 & 0.000 & 0.000 & 0.099 \end{pmatrix}$
TaCl	$\begin{pmatrix} 4.819 & 0.000 & 0.000 & 0.000 & 0.000 \\ 0.000 & 4.819 & 0.000 & 0.000 & 0.000 \\ 0.000 & 0.000 & 3.136 & 0.000 & 0.000 \\ 0.000 & 0.000 & 0.000 & 3.136 & 0.000 \\ 0.000 & 0.000 & 0.000 & 0.000 & 3.136 \end{pmatrix}$	$\begin{pmatrix} 0.628 & -1.452 & 0.000 & 0.000 & 0.000 \\ -1.452 & 2.305 & 0.000 & 0.000 & 0.000 \\ 0.000 & 0.000 & -0.137 & 0.000 & 0.000 \\ 0.000 & 0.000 & 0.000 & 1.500 & 0.000 \\ 0.000 & 0.000 & 0.000 & 0.000 & 1.500 \end{pmatrix}$
TaBr	$\begin{pmatrix} 6.649 & 0.000 & 0.000 & 0.000 & 0.000 \\ 0.000 & 6.649 & 0.000 & 0.000 & 0.000 \\ 0.000 & 0.000 & 3.830 & 0.000 & 0.000 \\ 0.000 & 0.000 & 0.000 & 3.830 & 0.000 \\ 0.000 & 0.000 & 0.000 & 0.000 & 3.830 \end{pmatrix}$	$\begin{pmatrix} 0.873 & -2.001 & 0.000 & 0.000 & 0.000 \\ -2.001 & 3.184 & 0.000 & 0.000 & 0.000 \\ 0.000 & 0.000 & -0.162 & 0.000 & 0.000 \\ 0.000 & 0.000 & 0.000 & 1.834 & 0.000 \\ 0.000 & 0.000 & 0.000 & 0.000 & 1.834 \end{pmatrix}$
YW	$\begin{pmatrix} 0.084 & 0.000 & 0.000 & 0.000 & 0.000 \\ 0.000 & 0.084 & 0.000 & 0.000 & 0.000 \\ 0.000 & 0.000 & 0.138 & 0.000 & 0.000 \\ 0.000 & 0.000 & 0.000 & 0.138 & 0.000 \\ 0.000 & 0.000 & 0.000 & 0.000 & 0.138 \end{pmatrix}$	$\begin{pmatrix} 0.010 & -0.026 & 0.000 & 0.000 & 0.000 \\ -0.026 & 0.040 & 0.000 & 0.000 & 0.000 \\ 0.000 & 0.000 & -0.007 & 0.000 & 0.000 \\ 0.000 & 0.000 & 0.000 & 0.065 & 0.000 \\ 0.000 & 0.000 & 0.000 & 0.000 & 0.065 \end{pmatrix}$

TABLE S5. Contribution from uniform strain: $K_{\mu'\gamma'}^{\mu\gamma}$ matrix in real space. The each 2×2 block correspondd to $\begin{pmatrix} K_{E_{g\theta}}^{E_{g\theta}} & K_{E_{g\theta}}^{E_{g\epsilon}} \\ K_{E_{g\epsilon}}^{E_{g\theta}} & K_{E_{g\epsilon}}^{E_{g\epsilon}} \end{pmatrix}$ of one JT center. The unit is meV.

	onsite
NaOs	$\begin{pmatrix} -14.040 & 0.000 & -0.438 & 4.712 & -0.438 & -4.712 & -8.599 & -0.000 \\ 0.000 & -14.040 & 4.712 & -5.878 & -4.712 & -5.878 & -0.000 & 2.283 \\ -0.438 & 4.712 & -2.061 & 2.927 & 1.102 & 1.019 & 0.664 & -0.766 \\ 4.712 & -5.878 & 2.927 & -5.441 & -1.019 & 0.518 & 1.271 & 0.956 \\ -0.438 & -4.712 & 1.102 & -1.019 & -2.061 & -2.927 & 0.664 & 0.766 \\ -4.712 & -5.878 & 1.019 & 0.518 & -2.927 & -5.441 & -1.271 & 0.956 \\ -8.599 & -0.000 & 0.664 & 1.271 & 0.664 & -1.271 & -7.131 & 0.000 \\ -0.000 & 2.283 & -0.766 & 0.956 & 0.766 & 0.956 & 0.000 & -0.371 \end{pmatrix}$
LiOs	$\begin{pmatrix} -15.532 & 0.000 & -0.296 & 5.283 & -0.283 & -5.283 & -9.481 & -0.001 \\ -0.000 & -15.532 & 5.285 & -6.399 & -5.302 & -6.414 & 0.002 & 2.781 \\ -0.285 & 5.309 & -2.184 & 2.928 & 1.437 & 1.452 & 0.567 & -0.951 \\ 5.311 & -6.415 & 2.928 & -5.565 & -1.452 & 0.272 & 1.959 & 1.149 \\ -0.298 & -5.292 & 1.421 & -1.432 & -2.184 & -2.933 & 0.563 & 0.947 \\ -5.311 & -6.399 & 1.431 & 0.287 & -2.923 & -5.565 & -1.957 & 1.146 \\ -9.449 & -0.002 & 0.567 & 1.920 & 0.571 & -1.923 & -7.255 & 0.000 \\ 0.001 & 2.754 & -0.937 & 1.134 & 0.940 & 1.138 & -0.000 & -0.493 \end{pmatrix}$
MgRe	$\begin{pmatrix} -12.159 & -0.000 & 0.924 & 4.532 & 0.924 & -4.532 & -6.925 & 0.000 \\ -0.000 & -12.159 & 4.532 & -4.309 & -4.532 & -4.309 & -0.000 & 3.541 \\ 0.924 & 4.532 & -2.168 & 1.969 & 1.211 & 1.244 & 1.343 & -1.320 \\ 4.532 & -4.309 & 1.969 & -4.441 & -1.244 & 1.387 & 1.168 & 1.255 \\ 0.924 & -4.532 & 1.211 & -1.244 & -2.168 & -1.969 & 1.343 & 1.320 \\ -4.532 & -4.309 & 1.244 & 1.387 & -1.969 & -4.441 & -1.168 & 1.255 \\ -6.925 & -0.000 & 1.343 & 1.168 & 1.343 & -1.168 & -5.577 & 0.000 \\ 0.000 & 3.541 & -1.320 & 1.255 & 1.320 & 1.255 & 0.000 & -1.031 \end{pmatrix}$
ZnRe	$\begin{pmatrix} -14.408 & 0.000 & 1.259 & 5.427 & 1.259 & -5.427 & -8.141 & -0.000 \\ 0.000 & -14.408 & 5.427 & -5.008 & -5.427 & -5.008 & 0.000 & 4.392 \\ 1.259 & 5.427 & -2.518 & 2.043 & 1.570 & 1.729 & 1.440 & -1.654 \\ 5.427 & -5.008 & 2.043 & -4.878 & -1.729 & 1.396 & 1.805 & 1.527 \\ 1.259 & -5.427 & 1.570 & -1.729 & -2.518 & -2.043 & 1.440 & 1.654 \\ -5.427 & -5.008 & 1.729 & 1.396 & -2.043 & -4.878 & -1.805 & 1.527 \\ -8.141 & 0.000 & 1.440 & 1.805 & 1.440 & -1.805 & -6.057 & -0.000 \\ -0.000 & 4.392 & -1.654 & 1.527 & 1.654 & 1.527 & -0.000 & -1.339 \end{pmatrix}$
TaCl	$\begin{pmatrix} -14.749 & 0.000 & -1.118 & 4.722 & -1.118 & -4.722 & -9.296 & -0.000 \\ 0.000 & -14.749 & 4.722 & -6.570 & -4.722 & -6.570 & -0.000 & 1.609 \\ -1.118 & 4.722 & -2.004 & 3.168 & 1.019 & 1.039 & 0.111 & -0.515 \\ 4.722 & -6.570 & 3.168 & -5.662 & -1.039 & -0.192 & 1.564 & 0.717 \\ -1.118 & -4.722 & 1.019 & -1.039 & -2.004 & -3.168 & 0.111 & 0.515 \\ -4.722 & -6.570 & 1.039 & -0.192 & -3.168 & -5.662 & -1.564 & 0.717 \\ -9.296 & -0.000 & 0.111 & 1.564 & 0.111 & -1.564 & -7.491 & -0.000 \\ -0.000 & 1.609 & -0.515 & 0.717 & 0.515 & 0.717 & -0.000 & -0.175 \end{pmatrix}$
TaBr	$\begin{pmatrix} -14.091 & -0.000 & -0.955 & 4.550 & -0.955 & -4.550 & -8.837 & 0.000 \\ -0.000 & -14.091 & 4.550 & -6.210 & -4.550 & -6.210 & -0.000 & 1.672 \\ -0.955 & 4.550 & -1.922 & 2.986 & 1.017 & 1.025 & 0.177 & -0.540 \\ 4.550 & -6.210 & 2.986 & -5.370 & -1.025 & -0.103 & 1.509 & 0.737 \\ -0.955 & -4.550 & 1.017 & -1.025 & -1.922 & -2.986 & 0.177 & 0.540 \\ -4.550 & -6.210 & 1.025 & -0.103 & -2.986 & -5.370 & -1.509 & 0.737 \\ -8.837 & -0.000 & 0.177 & 1.509 & 0.177 & -1.509 & -7.094 & 0.000 \\ 0.000 & 1.672 & -0.540 & 0.737 & 0.540 & 0.737 & 0.000 & -0.198 \end{pmatrix}$
YW	$\begin{pmatrix} -8.105 & -0.000 & 0.680 & 3.043 & 0.680 & -3.043 & -4.591 & -0.000 \\ -0.000 & -8.105 & 3.043 & -2.834 & -3.043 & -2.834 & 0.000 & 2.437 \\ 0.680 & 3.043 & -1.575 & 1.459 & 0.710 & 0.669 & 1.136 & -0.915 \\ 3.043 & -2.834 & 1.459 & -3.260 & -0.669 & 1.278 & 0.423 & 0.852 \\ 0.680 & -3.043 & 0.710 & -0.669 & -1.575 & -1.459 & 1.136 & 0.915 \\ -3.043 & -2.834 & 0.669 & 1.278 & -1.459 & -3.260 & -0.423 & 0.852 \\ -4.591 & 0.000 & 1.136 & 0.423 & 1.136 & -0.423 & -4.102 & 0.000 \\ -0.000 & 2.437 & -0.915 & 0.852 & 0.915 & 0.852 & 0.000 & -0.733 \end{pmatrix}$

TABLE S6. K matrix from IFCs: $K_{\mu'\gamma'}^{\mu\gamma}$ matrix in real space. The each 2×2 block correspondd to $\begin{pmatrix} K_{E_{g\theta}}^{E_{g\theta}} & K_{E_{g\theta}}^{E_{g\theta}} \\ K_{E_{g\theta}}^{E_{g\epsilon}} & K_{E_{g\epsilon}}^{E_{g\epsilon}} \end{pmatrix}$ of one JT center. The unit is meV .

	onsite
NaOs	$\begin{pmatrix} 75.840 & 0.000 & -1.059 & -1.040 & -1.059 & 1.040 & 0.743 & -0.000 \\ 0.000 & 75.840 & -1.040 & 0.143 & 1.040 & 0.143 & -0.000 & -1.659 \\ -1.059 & -1.040 & 75.840 & 0.000 & 0.743 & 0.000 & -1.059 & 1.040 \\ -1.040 & 0.143 & 0.000 & 75.840 & -0.000 & -1.659 & 1.040 & 0.143 \\ -1.059 & 1.040 & 0.743 & -0.000 & 75.840 & 0.000 & -1.059 & -1.040 \\ 1.040 & 0.143 & -0.000 & -1.659 & 0.000 & 75.840 & -1.040 & 0.143 \\ 0.743 & 0.000 & -1.059 & 1.040 & -1.059 & -1.040 & 75.840 & 0.000 \\ -0.000 & -1.659 & 1.040 & 0.143 & -1.040 & 0.143 & 0.000 & 75.840 \end{pmatrix}$
LiOs	$\begin{pmatrix} 71.103 & 0.000 & -1.366 & -1.249 & -1.366 & 1.249 & 0.799 & -0.000 \\ -0.000 & 71.103 & -1.249 & 0.077 & 1.249 & 0.077 & 0.000 & -2.087 \\ -1.366 & -1.258 & 71.112 & 0.003 & 0.798 & -0.002 & -1.366 & 1.259 \\ -1.258 & 0.084 & 0.003 & 71.108 & 0.010 & -2.091 & 1.247 & 0.072 \\ -1.368 & 1.258 & 0.798 & 0.002 & 71.112 & -0.003 & -1.366 & -1.259 \\ 1.258 & 0.084 & -0.010 & -2.091 & -0.003 & 71.108 & -1.247 & 0.072 \\ 0.810 & 0.000 & -1.373 & 1.243 & -1.373 & -1.243 & 71.106 & 0.000 \\ -0.000 & -2.095 & 1.255 & 0.079 & -1.255 & 0.079 & 0.000 & 71.114 \end{pmatrix}$
MgRe	$\begin{pmatrix} 71.577 & 0.000 & -2.285 & -1.809 & -2.285 & 1.809 & 0.849 & -0.000 \\ 0.000 & 71.577 & -1.809 & -0.196 & 1.809 & -0.196 & -0.000 & -3.329 \\ -2.285 & -1.809 & 71.577 & 0.000 & 0.849 & -0.000 & -2.285 & 1.809 \\ -1.809 & -0.196 & 0.000 & 71.577 & 0.000 & -3.329 & 1.809 & -0.196 \\ -2.285 & 1.809 & 0.849 & 0.000 & 71.577 & 0.000 & -2.285 & -1.809 \\ 1.809 & -0.196 & 0.000 & -3.329 & 0.000 & 71.577 & -1.809 & -0.196 \\ 0.849 & 0.000 & -2.285 & 1.809 & -2.285 & -1.809 & 71.577 & 0.000 \\ 0.000 & -3.329 & 1.809 & -0.196 & -1.809 & -0.196 & 0.000 & 71.577 \end{pmatrix}$
ZnRe	$\begin{pmatrix} 69.865 & 0.000 & -2.639 & -2.244 & -2.639 & 2.244 & 1.248 & 0.000 \\ 0.000 & 69.865 & -2.244 & -0.047 & 2.244 & -0.047 & -0.000 & -3.934 \\ -2.639 & -2.244 & 69.865 & 0.000 & 1.248 & 0.000 & -2.639 & 2.244 \\ -2.244 & -0.047 & 0.000 & 69.865 & -0.000 & -3.934 & 2.244 & -0.047 \\ -2.639 & 2.244 & 1.248 & 0.000 & 69.865 & 0.000 & -2.639 & -2.244 \\ 2.244 & -0.047 & -0.000 & -3.934 & 0.000 & 69.865 & -2.244 & -0.047 \\ 1.248 & -0.000 & -2.639 & 2.244 & -2.639 & -2.244 & 69.865 & 0.000 \\ -0.000 & -3.934 & 2.244 & -0.047 & -2.244 & -0.047 & 0.000 & 69.865 \end{pmatrix}$
TaCl	$\begin{pmatrix} 33.319 & 0.000 & -0.297 & -0.247 & -0.297 & 0.247 & 0.130 & -0.000 \\ 0.000 & 33.319 & -0.247 & -0.012 & 0.247 & -0.012 & -0.000 & -0.439 \\ -0.297 & -0.247 & 33.319 & 0.000 & 0.130 & -0.000 & -0.297 & 0.247 \\ -0.247 & -0.012 & 0.000 & 33.319 & -0.000 & -0.439 & 0.247 & -0.012 \\ -0.297 & 0.247 & 0.130 & -0.000 & 33.319 & 0.000 & -0.297 & -0.247 \\ 0.247 & -0.012 & -0.000 & -0.439 & 0.000 & 33.319 & -0.247 & -0.012 \\ 0.130 & 0.000 & -0.297 & 0.247 & -0.297 & -0.247 & 33.319 & 0.000 \\ -0.000 & -0.439 & 0.247 & -0.012 & -0.247 & -0.012 & 0.000 & 33.319 \end{pmatrix}$
TaBr	$\begin{pmatrix} 30.482 & 0.000 & -0.306 & -0.255 & -0.306 & 0.255 & 0.136 & 0.000 \\ -0.000 & 30.482 & -0.255 & -0.011 & 0.255 & -0.011 & 0.000 & -0.453 \\ -0.306 & -0.255 & 30.482 & 0.000 & 0.136 & -0.000 & -0.306 & 0.255 \\ -0.255 & -0.011 & -0.000 & 30.482 & -0.000 & -0.453 & 0.255 & -0.011 \\ -0.306 & 0.255 & 0.136 & -0.000 & 30.482 & 0.000 & -0.306 & -0.255 \\ 0.255 & -0.011 & -0.000 & -0.453 & -0.000 & 30.482 & -0.255 & -0.011 \\ 0.136 & 0.000 & -0.306 & 0.255 & -0.306 & -0.255 & 30.482 & 0.000 \\ -0.000 & -0.453 & 0.255 & -0.011 & -0.255 & -0.011 & -0.000 & 30.482 \end{pmatrix}$
YW	$\begin{pmatrix} 74.949 & 0.000 & -1.860 & -1.509 & -1.860 & 1.509 & 0.753 & 0.000 \\ -0.000 & 74.949 & -1.509 & -0.118 & 1.509 & -0.118 & 0.000 & -2.731 \\ -1.860 & -1.509 & 74.949 & 0.000 & 0.753 & 0.000 & -1.860 & 1.509 \\ -1.509 & -0.118 & -0.000 & 74.949 & 0.000 & -2.731 & 1.509 & -0.118 \\ -1.860 & 1.509 & 0.753 & 0.000 & 74.949 & 0.000 & -1.860 & -1.509 \\ 1.509 & -0.118 & -0.000 & -2.731 & -0.000 & 74.949 & -1.509 & -0.118 \\ 0.753 & 0.000 & -1.860 & 1.509 & -1.860 & -1.509 & 74.949 & 0.000 \\ -0.000 & -2.731 & 1.509 & -0.118 & -1.509 & -0.118 & -0.000 & 74.949 \end{pmatrix}$